Astron. Astrophys. 205, 309–327 (1988)

ASTRONOMY AND ASTROPHYSICS

The dynamics of coorbital satellite systems

H. Salo[1,2,★] **and C.F. Yoder**[1]

[1] Jet Propulsion Laboratory, 4800 Oak Grove Drive, Pasadena, CA 91109, USA
[2] Department of Astronomy, University of Oulu, SF-90570 Oulu, Finland

Received December 17, 1987; accepted February, 8, 1988

Summary. The dynamical behavior of N coorbital satellites, moving with the same average mean motion around a primary has been studied both analytically and in terms of numerical integrations for $2 \leq N \leq 9$ satellites. Simplified dynamical equations have been used to determine the different stationary configurations and their local stability against infinitesimal perturbations. The motion is reduced to angular separations between satellites and is accurate to the first order in satellite to primary mass ratio. The ring of equally spaced identical satellites is found to be locally unstable for $N \leq 6$, while for $2 \leq N \leq 8$ there exists another, stable compact stationary configuration, with separations $\leq 60°$ between adjacent satellites. For $N \geq 7$ the equally spaced configuration becomes locally stable, and for $N \geq 9$ it is the only stationary configuration. Exact integrations confirm these results, and also allow study of finite amplitude oscillations. The motion becomes chaotic for large amplitude perturbations. However, the chaotic motion fills a restricted region of phase space whose outer boundary is determined by the *maximum velocity curve* (mvc). This bounding curve is derived from the simplified equations using total energy and angular momentum conservation to obtain extrema in the kinetic and potential energy of a pair of satellites. These conditions were further utilized in derivation of minimum separations, ϕ_{mvc} between pairs of satellites. Numerical integrations confirm Maxwell's result that particles may be ejected from the ring if $\phi_{\text{mvc}} \lesssim 5\phi_{\text{Hill}}$, where ϕ_{Hill} is the mutual sphere of influence between a pair of satellites. Application to the coorbiter satellite pair of Saturn indicates that a triplet consisting of Janus (S10) and two satellites with the mass of Epimetheus (S11) would be unstable for the present total energy of the system.

Key words: celestial mechanics – numerical methods – planets and satellites – solar system

1. Introduction

The motion of N mutually gravitating satellites, confined to follow the same mean orbit, is an extremely simple system which can nevertheless exhibit complex behavior. The symmetrically spaced, many particle ring was originally examined by Maxwell (1890) in his Adams prize essay as a simple model for Saturn's rings. Although this model omits much of the dynamics which can occur when the ring has radial "width" (i.e. fills an annulus), Maxwell could use it to confirm that a multi-particle ring is stable in the limit $N \to \infty$ if the linear mass-density is sufficiently small. The present study concerns the orbital dynamics in the case of small N. Other researchers (Pendse, 1935; Willerding, 1986) have also expanded on Maxwell's work. From our point of view, Pendse's was the most interesting in that he added the indirect potential term to that obtained by Maxwell. This term results from the shifting from the center of the mass coordinate system to the center of the primary (adopted by Maxwell), and largely governs the primary-satellite motion. Its inclusion has a dramatic effect on the number and stability of the stationary configuration for small N: although the symmetrically spaced ring is a stationary configuration, it is locally unstable for $N < 7$.

The 2-particle ring's stable (and stationary) configuration occurs when the particles are separated by 60° in longitude. For three identical particles, the stable configuration involves a separation of the outer particle from the central particle by about 47°.4. Our original purpose in reexamining this problem was to map out all the stationary configurations, with the hope that it might bear on how a ring might collapse to form, say, Saturn's coorbital satellites (Yoder et al., 1983). However, we initially had no insight that the number and complexity of the stationary configurations would be so rich. For example, the 7 particle ring has 5 distinct stationary configurations, two of which are locally stable. Moreover, each configuration has six distinct normal modes, with associated frequencies. Furthermore, we had little expectation that as one increases the amplitude of these normal modes, that the reasonably periodic stable motion becomes chaotic. Perhaps the most important result of this paper relates on our attempts to understand the onset and the underlaying symmetry of this chaotic motion. We have obtained a constraint, called the maximum velocity curve, which employs the energy and impulse constraints to obtain the extremal motion of a particle pair. This constraint is similar to one employed by Hénon (1970) in a study of the restricted three body problem.

The results presented in this paper are primarily obtained by using a simple first order theory, in which terms of the order $(m/M)^{3/2}$ are neglected, where m and M are masses of the satellite and the primary, respectively. The orbit eccentricity and inclination were also ignored. These simplified equations are used to determine the stationary states and their stability matrixes.

Send offprint requests to: H. Salo
★ NRC Research Associate

These simple equations are also numerically integrated, using different initial conditions, and these results are compared with numerical integrations of the complete dynamical equations.

2. Simplified dynamical equations

The equations of motion for N mutually gravitating satellites, moving around a central mass in coplanar orbits, can be written in the form (see e.g. Yoder et al., 1983; Brown and Shook, 1964),

$$\frac{d}{dt}\left(r_i^2\frac{d\theta_i}{dt}\right)=\sum_{\substack{j=1\\ j\neq i}}^{N}\frac{\partial F_{ij}}{\partial\theta_i}, \tag{1}$$

$$\frac{d^2r_i}{dt^2}-r_i\left(\frac{d\theta_i}{dt}\right)^2=-\frac{\gamma M}{r_i^2}+\sum_{\substack{j=1\\ j\neq i}}^{N}\frac{\partial F_{ij}}{\partial r_i}, \tag{2}$$

where

$$F_{ij}=\gamma m_j\left\{\frac{1}{\Delta_{ij}}-\frac{r_i}{r_j^2}\cos(\theta_i-\theta_j)\right\}, \tag{3}$$

$$\Delta_{ij}^2=r_i^2+r_j^2-2r_ir_j\cos(\theta_i-\theta_j). \tag{4}$$

The polar coordinates (r,θ) are referred to the center of mass of the primary, which gives rise to the indirect terms $\sim\cos(\theta_i-\theta_j)$ in the forcing functions F_{ij}. Satellite masses are denoted by m_i, while M stands for the central mass and γ for the gravitational constant.

Denote the average mean motion of satellites by n_0 and the mean orbit radius by a_0. The deviations δn_i and δr_i, caused by the mutual interactions, are related as follows:

$$d\theta_i/dt=n_0+\delta n_i, \tag{5}$$

$$r_i=a_0(1-\tfrac{2}{3}\delta n_i/n_0)+\delta r_i, \tag{6}$$

where the first term on the right hand side of Eq. (6) follows from Kepler's third law. Substitution of Eqs. (5) and (6) into (1) and (2) yields

$$-\frac{1}{3}a_0^2\frac{d}{dt}(\delta n_i)+2n_0a_0\frac{d}{dt}(\delta r_i)=\sum_{\substack{j=1\\ j\neq i}}^{N}\frac{\partial F_{ij}}{\partial\theta_i}, \tag{7}$$

$$\frac{d^2}{dt^2}(\delta r_i)-\frac{2}{3}\frac{a_0}{n_0}\frac{d^2}{dt^2}(\delta n_i)-3n_0^2\delta r_i=\sum_{\substack{j=1\\ j\neq i}}^{N}\frac{\partial F_{ij}}{\partial r_i}, \tag{8}$$

where only the first order terms in δn_i and δr_i are retained on the left hand side. It can be shown (e.g. Yoder et al., 1983) that due to the Keplerian properties of the central force field, the deviations $\delta r_i/a_0$ are smaller by a factor $\sim(m/M)^{1/2}$ than $\delta n_i/n_0$'s (here m is a typical mass of a satellite). Therefore, to obtain expressions which are accurate to $O(m/M)$, the terms $\sim\delta r$ in Eq. (7) can be omitted. With the same accuracy, $F(r_i,r_j,\theta_i-\theta_j)$ can be replaced by $F(a_0,a_0,\theta_i-\theta_j)$, so that

$$-\tfrac{1}{3}d(\delta n_i)/dt=-n_0^2\sum_{\substack{j=1\\ j\neq i}}^{N}\mu_j\sin\theta_{ij}\left\{\frac{1}{8|\sin(\theta_{ij}/2)|^3}-1\right\} \tag{9}$$

where $\mu_j=m_j/M$, and $\theta_{ij}=\theta_i-\theta_j$. According to this approximate dynamical equation, the apparent force between a pair of satellites is repulsive for separations less than 60°. The stationary configurations correspond to the case where all the $d/dt(\delta n_i)$'s simultaneously vanish.

An energy integral follows from Eq. (9): multiplying both sides with $\mu_i\,\delta n_i$ for each i, summing over i, and finally integrating with respect to time, one obtains

$$E=T+V=-\frac{1}{6}\sum_{i=1}^{N}\mu_i(\delta n_i)^2-\frac{n_0^2}{2}\sum_{\substack{i,j\\ i\neq j}}^{N}\mu_i\mu_j\left\{\frac{1}{2|\sin(\theta_{ij}/2)|}-\cos\theta_{ij}\right\}. \tag{10}$$

The negative sign of the equivalent kinetic energy T follows from the almost Keplerian properties of the orbits, Eq. (5) and (6).

In the case of two satellites, the entire relative motion can be derived from Eq. (10), in terms of the difference angle $\phi=\theta_2-\theta_1$. An equivalent representation to Eq. (10) is (Yoder et al., 1983)

$$E=-\tfrac{1}{6}\dot{\phi}^2-n_0^2(\mu_1+\mu_2)\left\{\frac{1}{2|\sin(\phi/2)|}-\cos\phi\right\}. \tag{11}$$

The time evolution of ϕ could then be determined by a simple quadrature. The extrema of $V(\phi)$ correspond to the stationary solutions. Two basic types of motion are possible, depending on the initial conditions: stable librations around $\phi=\pm60°$, or horseshoe orbits extending around both $-60°$ and $60°$. The solution $\phi=180°$ is unstable, and corresponds to the limiting tadpole orbit separating the two regions of stable motion. The fact that a maximum of gravitational potential corresponds to a stable configuration results from T being negative definite.

For $N>2$ the situation is more complex, due to the large number of dependent variables: the energy condition is not sufficent to determine all the difference angles. However, for $N=3$ some progress can be made by plotting the mutual gravitational potential as a function of angular separations, $\phi_i=\theta_{i+1}-\theta_i$. For convenience, assume $\theta_1<\theta_2<\theta_3$, and define new variables,

$$\begin{aligned}&\alpha=(\phi_1+\phi_2)/2=(\theta_3-\theta_1)/2; && 0°<\alpha<180°,\\ &\beta=(\phi_1-\phi_2)/2=\theta_2-(\theta_3+\theta_1)/2; && -\alpha<\beta<\alpha,\end{aligned} \tag{12}$$

so that α corresponds to the mean interparticle separation, while β describes the deviation of the middle particle from the equidistant position. Figure 1a shows the potential surface as a function of α and β for identical satellite masses. The interpretation in terms of ϕ_i's is shown in the contour plot, Fig. 1b.

The potential has now three identical maxima: one of them is located at $(\alpha,\beta)=(47.^\circ4,0°)$, while the other two correspond to a cyclic permutation of particle indexes. The equally spaced configuration, $(120°,0°)$ is again a local minimum. In addition, V has three saddle points, at $(138.^\circ8,0°)$ and at the corresponding cyclic permutations. While all of these extrema are stationary configurations, it is clear from the analogy to the case $N=2$, that stable librations are possible only in the vicinity of the local maxima of V, corresponding to $47.^\circ4$ separations between adjacent satellites.

For $N>3$ there is no simple way to plot the potential. Instead, we shall probe the form of the V by solving numerically for the stationary solutions of Eq. (9). This gives the angular separations corresponding to the extrema of V. An eigenmode analysis is then performed in order to study the stability of these solutions (Sect. 3). For obvious reasons we concentrate on the case of identical satellites. A few numerical integrations are described in Sect. 4, in order to interpret and extend the results of the eigenmode analysis. Also, a maximum velocity curve will be defined

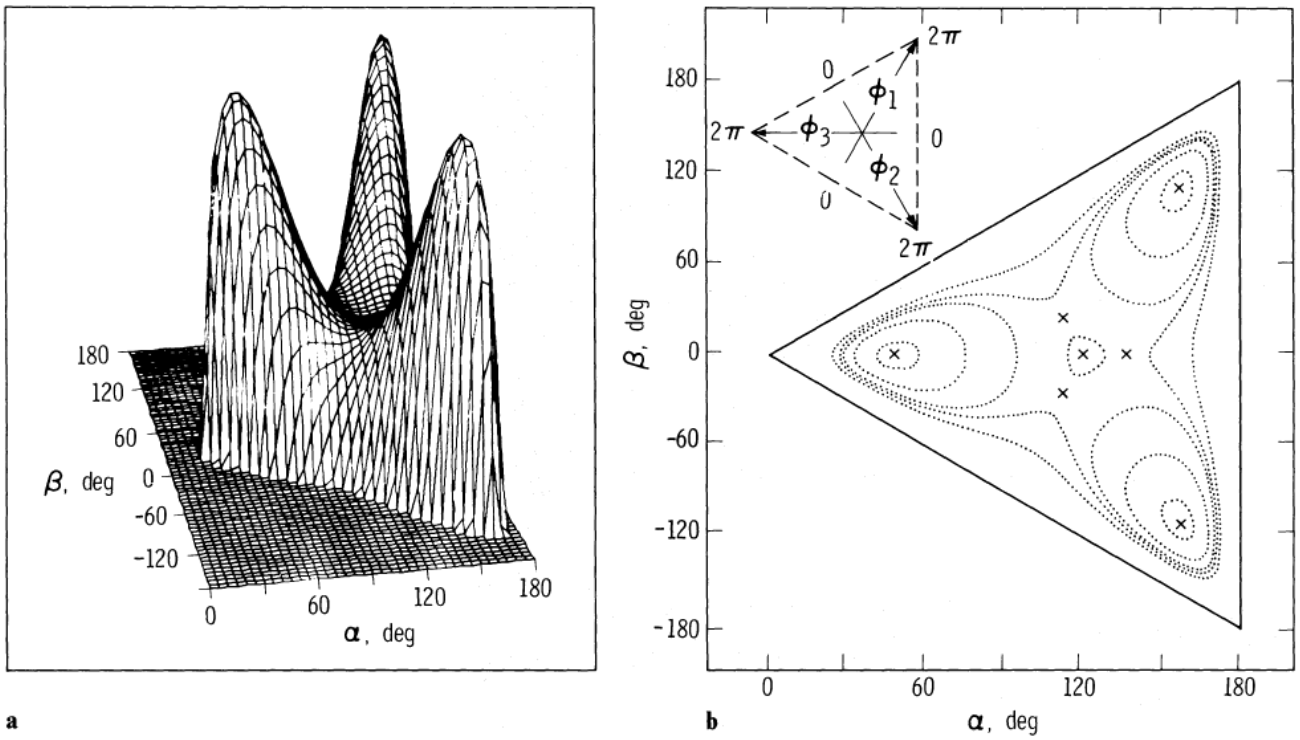

a b

Fig. 1. a The mutual potential energy for a 3 satellite ring, shown as a function of $\alpha = \frac{1}{2}(\phi_1 + \phi_2)$ and $\beta = \frac{1}{2}(\phi_1 - \phi_2)$. The three maxima correspond to stable 47°.4 separation between adjacent satellites. **b** Corresponding contour plot. The interpretation in terms of difference angles ϕ_i is also shown

and derived from Eq. (10), and is used to determine the conditions necessary for the onset of chaotic motion and the general character of that chaos in the phase space. Finally, a brief discussion about the effects of unequal satellite masses is given (Sect. 5).

3. Stationary configurations

Numerical search for the stationary configurations of identical coorbital satellites revealed the existence of three distinct types of solutions (Figs. 2 and 3). The first one, Type I, corresponds

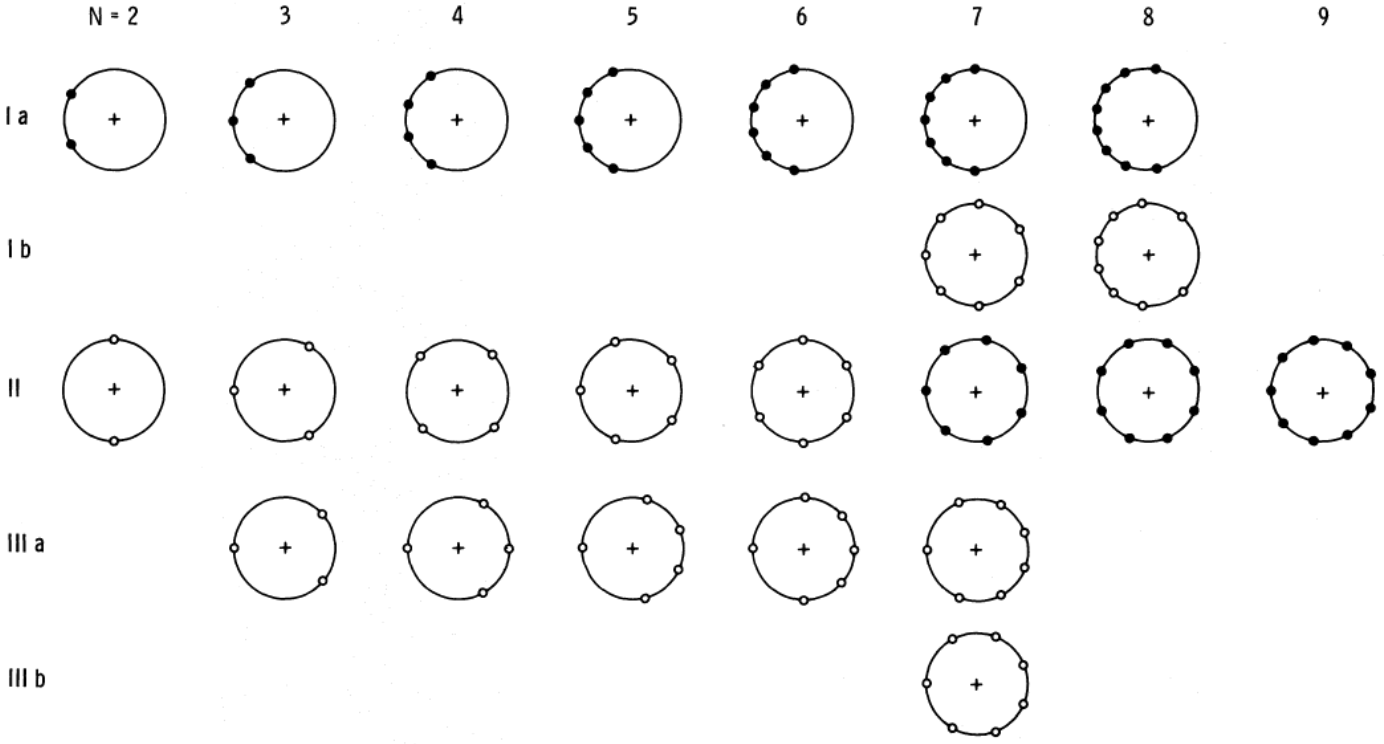

Fig. 2. Different stationary configurations for $N = 2$ to 9 identical satellites. Filled circles denote stable configuration

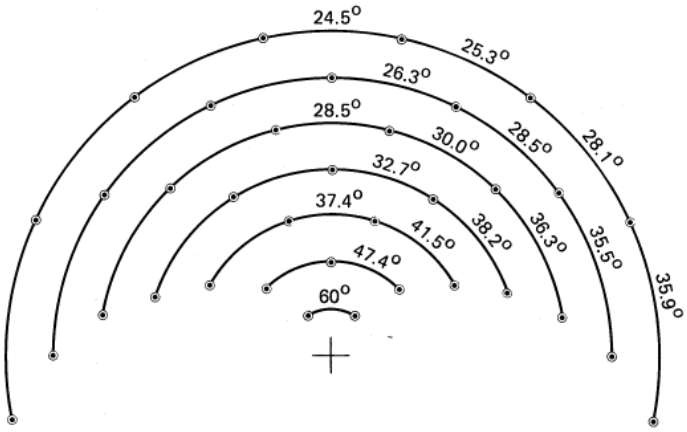

Fig. 3. The angular separations for the stable compact configuration (Type I), for $2 \leq N \leq 8$ satellites

to an equilibrium where all the N satellites are concentrated more or less to the same side of the common orbit, with mutual separations less than 60° between two subsequent satellites. In this case the mutual repulsive forces (in the non-inertial frame) between the nearest satellites are balanced by the attraction from the satellites further than 60° apart. The second type of solutions is the trivial one corresponding to equally spaced satellites. Finally, in the Type III configuration $N-1$ satellites revolve in one side, while the remaining one is situated diametrically opposite to the rest. The different solutions are collected to Table 1, for $2 \leq N \leq 9$. As can be seen Type I solutions were found only for $N \leq 8$, whereas Type III solutions were further confined to interval $3 \leq N \leq 7$. For $N \geq 9$ the trivial solution is apparently the only one. In the case $N = 7$ there exists another variation from both Type I and Type III solutions, corresponding to the same general type of configuration but with a somewhat wider separation between satellites. These additional solutions are de-

Table 1. The stationary configurations for $N = 2$ to 9 identical coorbital satellites. The angular position are given (centered at 180°), together with the $N-1$ non-zero eigenvalues (in units μn_0^2), and the gravitational potential energy (in units of $\mu^2 n_0^2 a_0^2$)

N	Type	Positions	Eigenvalues	Energy
2	I	150.000	13.5000	−0.5000
		210.000		
2	II	90.000	−5.2500	−1.5000
		270.000		
3	I	132.639	14.9292	−1.8971
		180.000	38.0240	
		227.361		
3	II	60.000	−2.3349	−3.2321
		180.000	−2.3349	
		300.000		
3	III	41.235	−5.2259	−3.2000
		180.000	4.4151	
		318.765		
4	I	119.824	15.1258	−4.3607
		161.322	41.9465	
		198.678	73.3188	
		240.176		
4	II	45.000	−2.0680	−5.8284
		135.000	−2.0680	
		225.000	6.3640	
		315.000		
4	III	0.000	−5.7021	−5.7321
		60.000	4.4151	
		180.000	18.3672	
		300.000		
5	I	109.138	14.3233	−7.904
		147.340	43.6885	
		180.000	77.6988	
		212.660	119.6370	
		250.861		
5	II	36.000	−1.5500	−9.3819
		108.000	−1.5500	
		180.000	11.7139	
		252.000	11.7139	
		324.000		
5	III	23.046	−5.6570	−9.2611
		74.373	4.3344	
		180.000	21.4788	
		285.627	38.7894	
		336.954		
6	I	99.409	12.6011	−12.849
		135.719	43.2652	
		165.732	79.7551	
		194.268	122.2008	
		224.281	175.0269	
		260.591		
6	II	30.000	−0.8349	−13.9641
		90.000	−0.8349	
		150.000	17.9151	
		210.000	17.9151	
		270.000	21.7500	
		330.000		
6	III	0.000	−4.7475	−13.8832
		40.520	3.0848	
		88.044	21.6443	
		180.000	40.2072	
		271.956	62.4878	
		319.480		
7	I	89.724	9.9030	−18.9674
		125.187	40.2976	
		153.722	76.2866	
		180.000	119.4734	
		206.278	172.0589	
		234.813	234.7970	
		270.276		
7	Ib	30.275	−0.0984	−19.6337
		85.822	0.0310	

Table 1 (continued)

N	Type	Positions	Eigenvalues	Energy
		134.599	20.9732	
		180.000	25.0937	
		225.400	34.3875	
		274.179	45.5621	
		329.727		
7	II	25.716	0.0426	−19.6334
		77.144	0.0426	
		128.572	24.8002	
		180.000	24.8002	
		231.428	33.4815	
		282.856	33.4815	
		334.284		
7	IIIb	22.063	−0.9081	−19.6337
		67.967	0.2070	
		119.609	17.8686	
		180.000	30.3248	
		240.392	46.1415	
		292.036	65.5383	
		337.933		
7	IIIa	19.791	−0.0623	−19.6332
		61.385	−0.0629	
		110.668	20.1549	
		180.000	25.4714	
		249.332	35.6241	
		298.615	48.0141	
		340.209		
8	I	78.506	5.8509	−26.3532
		114.408	33.4346	
		142.522	67.9744	
		167.770	108.6184	
		192.230	158.0008	
		217.478	217.1843	
		245.592	286.6259	
		281.494		
8	Ib	46.151	−2.0120	−26.5476
		95.643	5.1008	
		132.327	26.0675	
		164.513	46.9160	
		195.487	72.0685	
		227.673	102.6306	
		264.358	139.3835	
		313.849		
8	II	22.500	1.0587	−26.4389
		67.500	1.0587	
		112.500	32.2598	
		157.500	32.2598	
		202.500	46.5970	
		247.500	46.5970	
		292.500	51.7917	
		337.500		
9	II	20.000	2.1955	−34.4234
		60.000	2.1955	
		100.000	40.2157	
		140.000	40.2157	
		180.000	60.8835	
		220.000	60.8835	
		260.000	72.3510	
		300.000	72.3510	
		340.000		

noted by b) in Table 1. For $N = 8$, only the variation Ib) was found. In the case $N = 2$ and 3 these stationary configurations are the same as found already in Sect. 2.

In order to determine the stability of these configurations, we introduce a small perturbation to the stationary solution, $\theta = (\theta_i)_0 + \delta\theta_i$. Since at equilibrium $dn_i/dt = 0$ for all i, it follows that

$$\frac{d^2}{dt^2}\,\delta\theta_i = -3n_0^2 \sum_{\substack{j=1 \\ j\neq i}}^{N} H_{ij}(\delta\theta_i - \delta\theta_j), \qquad i = 1 \ldots N, \tag{13}$$

where

$$H_{ij} = \mu_j \cos(\theta_{ij})_0 \left\{ \frac{1}{8|\sin[(\theta_{ij})_0/2]|^3} - 1 \right\} - \frac{3\mu_j}{32} \frac{\sin^2(\theta_{ij})_0}{|\sin[(\theta_{ij})_0/2]|^5}, \tag{14}$$

while $(\theta_{ij})_0 = (\theta_i)_0 - (\theta_j)_0$. By denoting $\boldsymbol{X} = (\delta\theta_1, \ldots, \delta\theta_k, \ldots, \delta\theta_N)$, this is equivalent to $\ddot{\boldsymbol{X}} + \mathbf{A}\boldsymbol{X} = 0$, where the perturbation matrix $\mathbf{A}$ is obtained by collecting the multipliers of $\delta\theta_k$ in Eq. (13). In order to have a stable solution, all the eigenvalues λ_k (corresponding to square of the eigenfrequency) of the matrix $\mathbf{A}$ must be positive. For a positive eigenvalue the period of infinitesimal libration is $(\lambda_k\mu_i)^{-1/2}T_p$, where T_p is the orbital period. Notice that one of the eigenvalues is always zero, corresponding to an arbitrary rotation of the system as a whole. Having no physical interest it is discarded in the following analysis. Figure 4 depicts the eigenvalues of the perturbation matrix for different satellite configurations, as a function of N. For clarity, the eigenvalues corresponding to the same perturbation mode are connected by smooth curves. For Types I and III there is $N-1$ different (non-zero) eigenvalues, whereas for Type II solutions λ's form degenerate pairs. The eigenvalues are also shown in Table 1. An example of the related eigenvectors is shown in Fig. 5, for the case $N = 5$. For Types I and II the lowest curves in Fig. 4 correspond to a disturbance where the entire satellite configuration is contracting or expanding (in tangential direction) in phase, whereas for the uppermost curves the deviations of consecutive satellites occur at opposite directions. The same is true for the $N-2$ positive eigenvalues of Type III, which more or less describe the evolution of disturbances among the $N-1$ closely packed satellites. On the other hand, the negative eigenvalue of Type III corresponds to the movement of the remaining particle with respect to the other satellites.

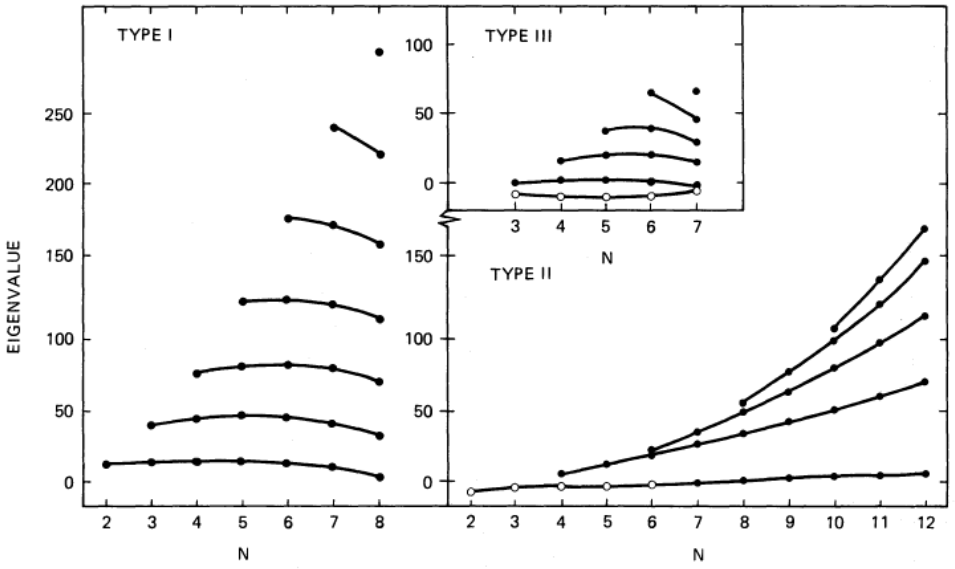

Fig. 4. The eigenvalues λ_k (in units μn_0^2) for Type I, II, and III stationary configurations. For clarity, the eigenvalues (circles) related to the same perturbation mode are connected with smooth lines for different N. Open circles mark negative eigenvalues, indicating unstable eigenmodes

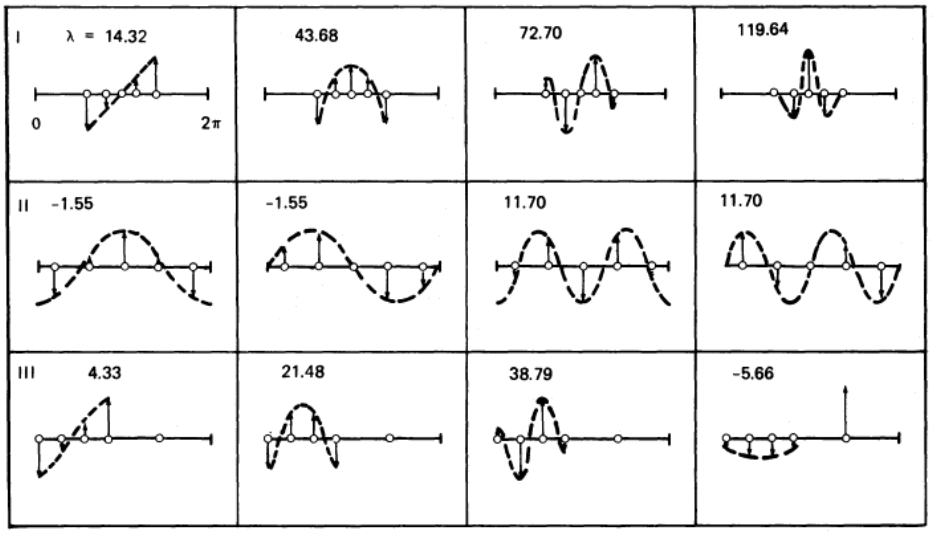

Fig. 5. The four different eigenmodes for $N = 5$ identical satellites, related to Type I, II, and III stationary configurations. The corresponding eigenvalue λ_k is also shown, in units of μn_0^2

The eigenvectors corresponding to the degenerate pairs of λ's (Type II configuration) can be represented by an arbitrary combination of the base vectors $\{\sin k\theta_i\}$ and $\{\cos k\theta_i\}$, where $2k$ is the number of nodes in the perturbation (see Fig. 5) and θ_i's are the equidistant positions. For the smallest λ-pair k equals 1, while for the largest pair (or single eigenvalue, in case N is even), $k = \text{int}(N/2)$. Notice that for the case $N =$ even, the $(\sin k\theta_i\}$ base vector vanishes for $k = N/2$, $\theta_i = 2\pi/N(i-1)$, so that there is no difference between the odd and even satellite numbers, although in the former case the fastest eigenmode is formally nondegenerate. For solutions of Type I and III the eigenvectors are also sinusoidal, but with the amplitude of oscillations generally largest for the innermost satellites (See Fig. 5).

For $N = 3$ ring the two eigenmodes have a simple geometrical interpretation. For example, for the compact configuration λ_1 corresponds to a symmetric oscillations of outer particles around a stationary middle satellite, $\delta n_2 - \delta n_1 = \delta n_3 - \delta n_2$, while λ_2 is related to an antisymmetric perturbation, $\delta n_2 - \delta n_1 = -(\delta n_3 - \delta n_2)$. In terms of the variables α and β, the former mode implies $\beta = 0$, while for the latter, α stays constant. Both these oscillation modes are stable: since the potential V falls steeper in the latter direction (see Fig. 1), antisymmetric oscillations have a higher frequency. The degeneracy of the equally spaced solution is a consequence of the fact there is no preferential direction to which the system evolves: the slope of V is the same in each direction around the unstable minimum.

An interesting point is the behavior of the slowest eigenmode for the equidistant solution, corresponding to the overall in-phase disturbances. For $N \leq 6$ the smallest eigenvalue is negative, indicating instability. For $N = 7$ it is very close to zero, whereas for $N \geq 8$ it is clearly positive. This indicates that the stability of the equidistant configuration depends strongly on the number of satellites. The Type I solutions, when they exist, are always stable. In terms of the mutual gravitational potential this means that for $N \leq 8$, V has N local maxima, analogous to Fig. 1, while for $N \geq 7$ the equally spaced configuration has also turned into a local maximum. All the other solutions have at least one unstable eigenmode and thus correspond to saddle

points of V. It is qualitatively clear why the compact solution seems to disappear for $N \geq 9$: according to Table 1 the energy difference $V_{II} - V_I$ decreases as $N > 4$, and is very close to zero for $N = 7$, 8. This indicates that all the $N + 1$ local maxima merge into one as $N \geq 9$. The appearance of the additional solutions for $N = 7$ and 8 is also related to the flatness of the potential surface.

The stability of the equally spaced satellites is exactly the same problem which was first addressed by Maxwell (1890; see also a recent rederivation by Willerding, 1986) in his essay concerning the stability of Saturn's rings. By studying small sinusoidal radial and tangential displacements from the equidistant positions, Maxwell derived a dispersion relation for the angular velocity of the perturbation, ω. Maxwell found that the motions most susceptible for the instability were the short wavelength tangential perturbations, corresponding to $k = N/2$. He concluded that unless the satellite masses exceed a critical limit, $\mu > 2.23/N^3$, ω stays real also for these perturbations, indicating no exponential growth of amplitude for any type perturbation. However, since Maxwell (1890) was mainly interested about the stability on the limit $N \to \infty$, he neglected the indirect part of the forcing function. This explains the disagreement with the eigenmode analysis, according to which rings composed of less than 7 satellites should be unstable independent of the satellite mass (see also Pendse, 1935). Also, in our analysis the unstable mode corresponds to the long wavelength perturbation, $k = 1$. On the other hand, Maxwell's critical mass limit appears to be related to the overlapping of the adjacent particle's spheres of influence. The eigenmode analysis, based on the assumption of basically Keplerian motions (see Eq. (6)) does not take into account this possibility (this case is considered later using numerical integrations of the exact equations).

We have extended Maxwell's original analysis to the limit of small N, by including the indirect terms. We have also corrected a few minor inaccuracies, like the omission of the satellite situated exactly on the opposite side (N = even) in the calculation of direct forces. The results are collected to Table 2, giving ω^2 calculated by Maxwell's method, both with and without indirect terms. (Actually, Maxwell's dispersion relation is a fourth-order polynomial on ω, so that there is a total of four roots, forming two pairs. Two of them correspond to perturbations having ω^2 very close to the square of the orbital angular velocity and are related to the precessions of inclined, eccentric particle orbits. These modes are omitted in our discussion. The difference between the remaining two roots comes from a slightly different velocity for a perturbation propagating in the direction of the orbital motion and against it. In the limit of vanishing satellite mass, for which the eigenmode analysis is valid, these roots are identical.)

Table 2. The square of the angular velocity of the long-wavelength perturbation (ω^2) for an equally spaced satellite configuration (corresponds to smallest eigenvalue), calculated with Maxwell's original method, and with the inclusion of the terms arising from indirect part of the forcing function (in units of μn_0^2)

N	Maxwell	Indirect
2	0	−5.250
3	2.165	−2.335
4	3.182	−2.068
5	5.950	−1.550
6	7.415	−0.835
7	10.543	0.042
8	12.309	1.0587
9	15.695	2.1955
10	17.689	3.4394
100	403.26	254.02
1000	6238.2	4738.9

According to Table 2 the agreement between Maxwell's method and the eigenmode analysis is complete (compare to Table 1, smallest eigenvalues for Type II configuration), once the indirect terms are properly taken into account. The agreement is related to the fact that the eigenvectors following from the perturbation analysis of Eq. (9) are exactly of the same form as assumed by Maxwell (1890). On the other hand, it is interesting to note the influence of the indirect term on the slowest eigenfrequency, especially for small N ($N \leq 6$) where the sign of the ω^2 differs for each case. Even if $N = 1000$, the ω^2 obtained by the modified method is about 25% smaller than with the omission of indirect forces. However, only the slowest mode is significantly affected. Therefore, Maxwell's original stability criterion for $N \to \infty$, related to fast modes, is not affected by the inclusion of the indirect terms.

4. Numerical integrations for identical masses

The above search for the stationary configurations and the eigenmode analysis of their stability gives only a limited understanding of the general behavior of the coorbital satellite ring. In the case of a stable configuration it assures the existence of a certain libration region, and describes the basic modes of small oscillations. However, the width of the stable region is not determined. Also, in the case of an unstable stationary configuration, the actual evolution of motion is left uncertain. The only way to extend the analysis is through numerical integration of orbits. The eigenmode analysis is still very useful in providing appropriate initial conditions for numerical investigations. All the numerical calculations are carried out by an ordinary RK4 integrator in double precision. Typically, the conservation of energy and angular momentum was satisfied within 10^{-11}.

According to eigenmode analysis, there are two basic libration modes for an $N = 3$ satellite ring: for the stable compact Type I configuration these correspond to either symmetric ($\delta n_2 - \delta n_1 = \delta n_3 - \delta n_2$; $M1$ mode) or antisymmetric ($\delta n_2 - \delta n_1 = -(\delta n_3 - \delta n_2)$; $M2$ mode) perturbation of the outer particles with respect to the middle one. Figure 6 depicts integrations of exact dynamical equations with initial conditions chosen according to these modes, as well as their combination $M1 + M2$. Three distinct types of plots are used here (and in following figures) in order to illustrate the motions: a) plots of satellite angular positions as a function of time, $\theta_i(t)$, in a reference frame rotating with the mean angular velocity of the system, $\sum \mu_i \delta n_i = 0$; b) (r, θ) plots in the same rotating frame; and c) plots of the system on the (α, β) plane (or equivalently, of all ϕ_i's). The units of numerical calculations are fixed by setting $a_0 = n_0 = 1$, so that the orbital period is 2π. For the mass ratio $\mu = 10^{-5}$, the periods of infinitesimal oscillations are 514 and 322 time units, for $M1$

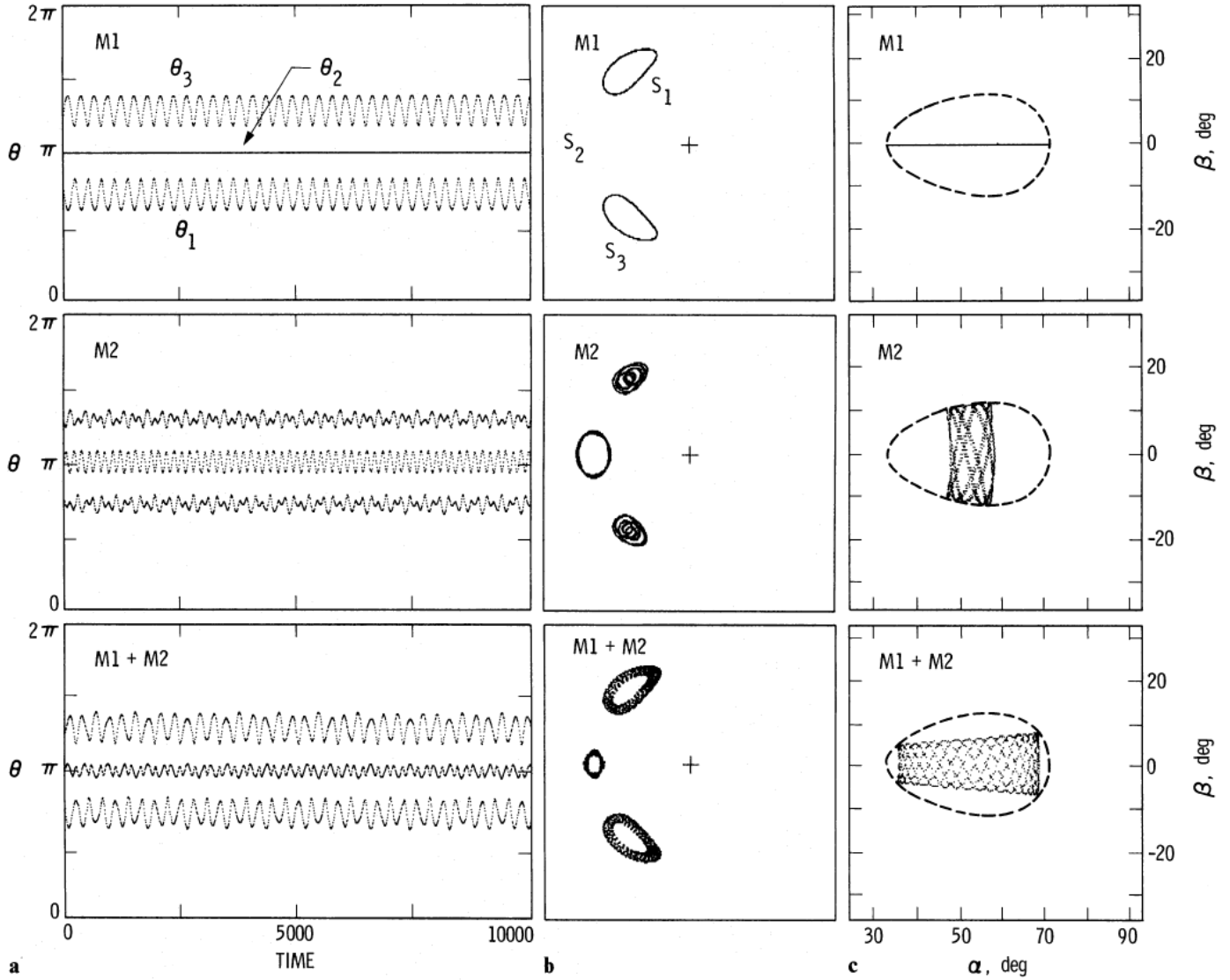

Fig. 6a–c. Results of numerical integrations of exact equations, for small amplitude oscillations ($E/V_I = 1.25$) around the stable Type I configuration of 3 identical satellites. Symmetric ($M1$) and antisymmetric ($M2$) initial perturbations, as well as their combination ($M1 + M2$) are studied in terms of angular positions (**a**), polar plots (**b**), radial deviations scaled by a factor 60, and (α, β) plots (**c**). The length of each integration is 20,000 time units, while $\mu = 10^{-5}$. The dashed lines in (c) indicate the contour $V(\alpha, \beta) = E$, inside which the motion is bounded

and $M2$ modes, respectively. In each integration, the initial radial displacements were adjusted with respect to δn_i's according to Eq. (6), to yield the same mean distance for all satellites. The strength of perturbation is described by $E/V_I = 1 + T/V_I$, where T is the kinetic energy associated with the perturbation, while V_I is the potential energy of the Type I configuration. In Fig. 6, $E/V_I = 1.25$.

According to numerical integrations, the eigenmodes and their frequencies derived from the simplified analysis are in excellent agreement with the actual dynamical behavior. In fact, the simplified equations were also integrated, giving practically identical behavior as compared to exact equations. For infinitesimal oscillations both basic modes, $M1$ and $M2$, lead to closed loops in the rotating coordinate frame. The corresponding images in the (α, β) plane are horizontal and vertical lines, respectively. However, although the symmetric $M1$ mode remains distinct also for finite perturbations, the antisymmetric mode $M2$ cannot (Fig. 6). This can be interpreted as follows. If Eq. (9) is written in terms of α and β, it follows that (assuming equal masses)

$$\ddot{\alpha}/3n_0^2 = G(2\alpha) + \tfrac{1}{2}\{G(\alpha - \beta) + G(\alpha + \beta)\}\,, \tag{15}$$

$$\ddot{\beta}/3n_0^2 = \tfrac{3}{2}\{G(\alpha + \beta) - G(\alpha - \beta)\}\,, \tag{16}$$

where $G(x)$ is a shorthand notation for $\sin x\{|2\sin x|^{-3} - 1\}$. Therefore, $\ddot{\beta}$ always vanishes for $\beta = 0$, independent of α. On the other hand, in general $\ddot{\alpha} \neq 0$ for $\beta \neq 0$. As a result, α can not stay constant if the $M2$ mode is excited by non-infinitesimal amount, which leads to complicated trajectories in the $r_i(\theta_i)$ as well as the (α, β) plane. This tendency for mixing of modes has important consequences if E/V_I is increased.

In order to study large perturbations to more detail, another series of integrations was carried out for the symmetrical mode, with larger initial E/V_I (Fig. 7). Exact equations were integrated over 50,000 time units, starting again from the Type I positions. As E/V_I is increased the middle particle can no longer remain

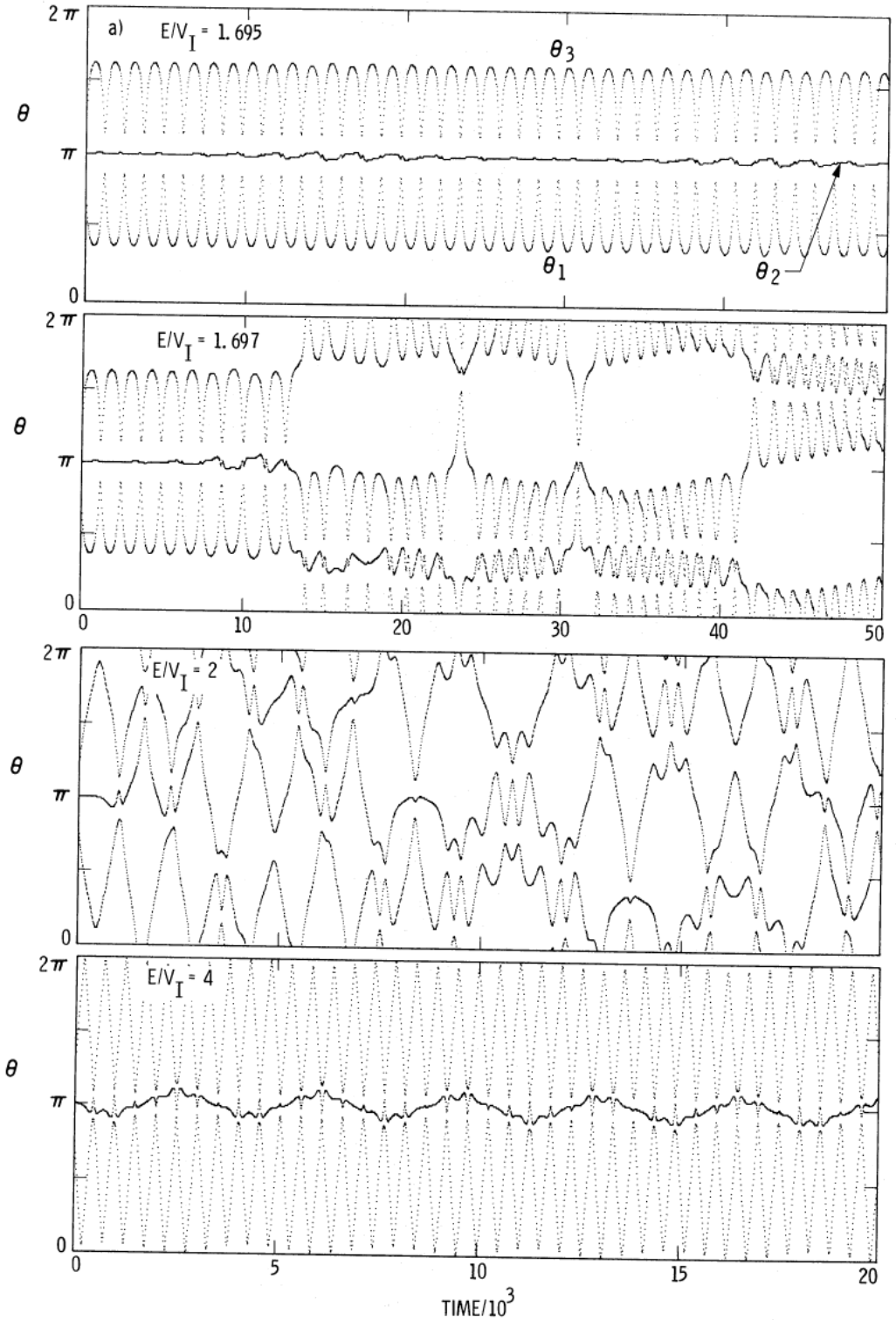

Fig. 7a

Fig. 7a–c. Same as Fig. 6, except that larger perturbations are studied for the symmetric $M1$ mode. In polar plots (**b**), the scale of the plots for individual particles is $\frac{1}{2}$ of the combined plot

stationary, but starts to perform finite oscillations, corresponding to excitement of $M2$ mode (Fig. 7). This follows from the terms proportional to $\mu^{3/2}$, ignored in the approximation leading to Eq. (9). For example, in the symmetric mode with $\alpha < 120°$, due to the mutual interactions, the middle satellite always feels a slightly larger radial attraction than the other two particles. It tries to balance this by adjusting its angular velocity. Hence, the variable β, describing the amount of antisymmetric mode, tends to grow from its initial zero value. However, according to Eq. (16) $\Delta\ddot{\beta}/\Delta\beta \leq 0$ for $\alpha \lesssim 106°.8$ and the deviations are damped (proportionally to μ). Therefore, the fluctuations stay bounded. On the other hand, if $\alpha \gtrsim 106°.8$, the deviations start to grow

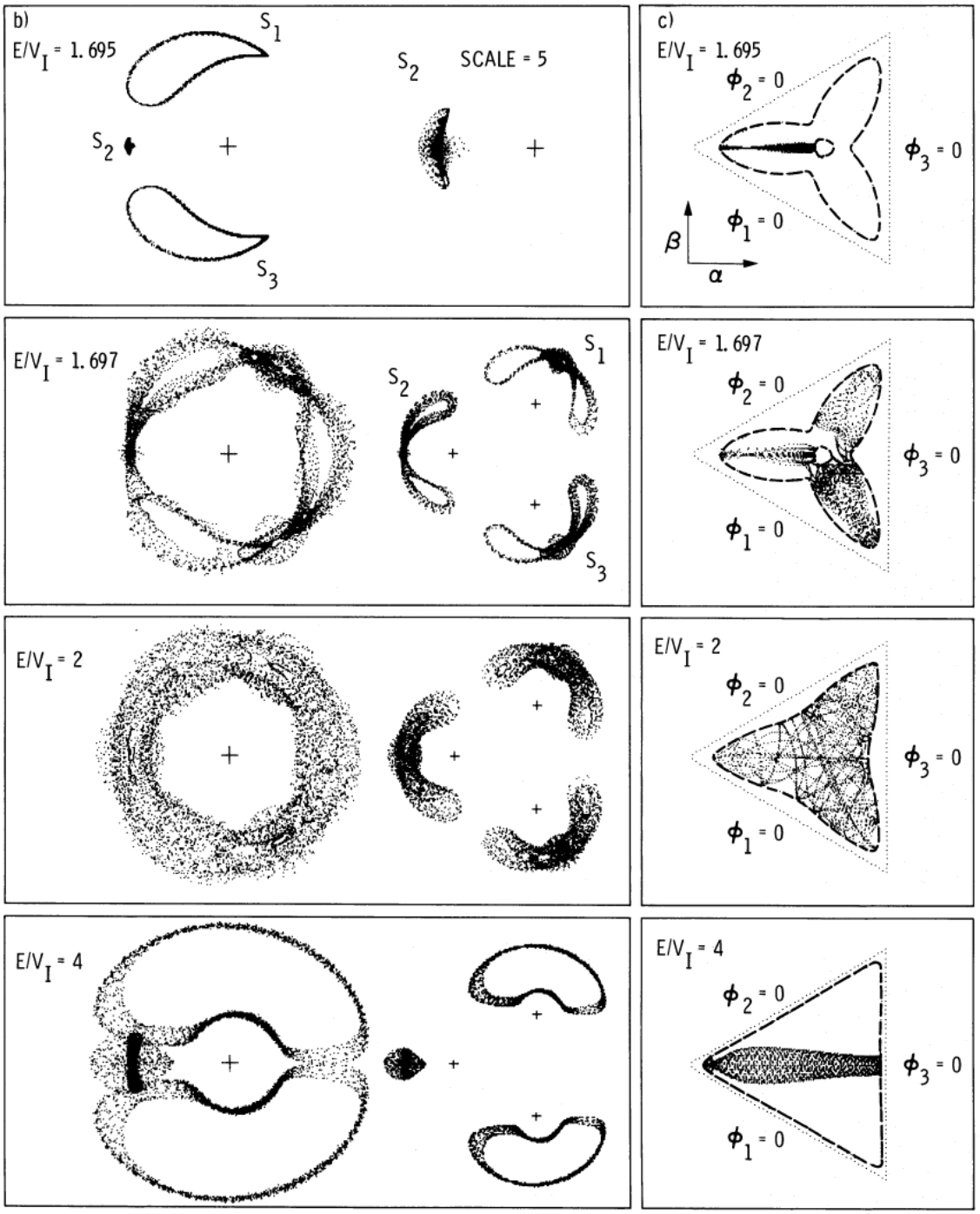

Fig. 7b and c

during that part of the orbits were this critical separations is exceeded. At first this results only in a curious double feature in the region occupied by the middle particle, together with the thickening of the region of the orbits of the outer particles (Fig. 7, $E/V_I = 1.695$). According to Fig. 6, this is the typical feature of the antisymmetric mode.

As E/V_I is further increased (Fig. 7, $E/V_I = 1.697$), the motion becomes rapidly unstable against the growth of the $M2$ mode, since the particles always spend most of their time close to 120° separations. After a few librations, instead of completing the symmetric oscillation with respect to the initially stationary particle, the system collapses towards either one of the other two satellites. Subsequent expansion with respect to the new middle particle leads once more to the unstable region, and as a consequence sooner or later a new shift in the role of the satellites is observed. Clearly, this exchange of identities occurs in a chaotic manner, although during a short integration one oscillation mode can seem to dominate. However, as E/V_I is increased the (α, β) plane is almost uniformly filled with trajectories (Fig. 7, $E/V_I = 2$).

The transition between the periodic and chaotic behavior is very sharp, taking place for energies between $E/V_I = 1.695$ and

1.697. The same transition was also observed in two otherwise identical integrations, except that the particles started with zero relative velocities from $\alpha = 112°.5$ and 113°.

It is interesting to note that for still larger E/V_I ($\gtrsim 3.5$), the initial identity of the satellites is once more retained, in the sense that the middle particle performs a unique oscillation, while the outer particles perform motion analogous to the horseshoe orbits for $N = 2$ (Fig. 7, $E/V_I = 4$). For extremely large perturbation the behavior becomes very complicated: since the minimum separations decrease with increasing E/V_I, the particles eventually penetrate into their mutual sphere of influence. The close encounters can lead to an escape or the passing of the satellites, although this is not allowed by the simplified description (Eqs. 7–9) which prevent particles from leaving the ring or exchanging their relative positions. We shall briefly return to this problem later.

It is useful to interpret the above described onset of chaotic motion in the light of the 3-particle potential (Fig. 1). Since the kinetic energy is a negative definite quantity, the system is confined to stay below the potential surface. Figures 6c and 7c shows the allowed region in (α, β) plane, bounded by the curve $V(\alpha, \beta) = E$. For small amplitude librations around the Type I stationary configuration, $E/V_I \geq 1$, the allowed portion of (α, β) plane consists of three separate regions, and the system remains safely in the vicinity of the initial configuration (Fig. 6c; only one of the allowed regions shown). For larger E/V_I (Fig. 7) these permitted regions widen, until at certain energy, ($E = V_{III}$; $E/V_I = 1.689$), they finally merge, leaving an isolated non-allowed region around the equally spaced configuration. Hence, if $E/V_I \geq V_{III}/V_I$, the system can pass around the 120° potential minimum, and start performing oscillations inside any of the three peaks. As can be seen from the case $E/V_I = 1.697$, this indeed happens and each particle seems to perform statistically similar orbit regardless of the nonidentical initial conditions. For $E/V_I > V_{II}/V_I$, the motion is energetically allowed to pass through any point inside the outer contours corresponding to $V(\alpha, \beta) = E$. However, as was demonstrated by the integrations with $E/V_I = 4$, this does not necessarily happen. This can be explained by noting that due to the large $|T|$ the minimum of V at 120° separation cannot significantly slow down the initially large relative velocities, and there is not enough time for the $M2$ mode to grow sufficiently to break the dominant symmetric mode.

It is important to note that although the destruction of the strictly symmetrical motion is related to the terms ignored in the approximation leading to simplified equations, the phenomenon itself takes place regardless of the satellite mass. This follows from the fact that the terms ignored in Eq. (9) are not necessary to keep up the instability, but simply trigger the mixing of the two modes, which in itself is well described by Eqs. (15) and (16) for $N = 3$ (see Fig. 6). This was further verified by additional integrations performed with $\mu = 10^{-6}$ and 10^{-7}, starting from symmetric 113° separations with zero relative velocities. Both integrations led to the exchange of particle identities within the first few librations. In fact, even in the absence of any $\mu^{3/2}$ terms, small external perturbations would probably disturb the symmetric motion.

Although the bounds set by the total energy give a sufficient "geometric" explanation for the behavior of three particle ring, we can proceed still further by utilizing the conservation of angular momentum. In what follows we attempt to set further limits on the allowed trajectories, in the phase space $(\phi_i, \dot{\phi}_i)$. In order to do this we search for the maximum of $\dot{\phi}_k$, subject to conditions

$$\sum_{i=1}^{N} \mu_i \delta n_i = 0, \tag{17}$$

$$\sum_{i=1}^{N} \mu_i \delta n_i^2 = -6T. \tag{18}$$

With the help of Langrange multipliers (l_1, l_2) this is equivalent of determining the extremum of

$$g = (\delta n_{k+1} - \delta n_k)^2 + l_1 \sum_{i=1}^{N} \mu_i \delta n_i + l_2 \left(\sum_{i=1}^{N} \mu_i \delta n_i^2 + 6T \right) \tag{19}$$

by setting the partials $\partial g / \partial n_k = 0$, and then solving these N equations together with the conditions (17) and (18) for the $N + 2$ unknowns, δn_k, l_1, and l_2. The maximum of $\dot{\phi}_k^2$ is obtained when $\delta n_{k+1} = -\mu_k / \mu_{k+1} \, \delta n_k$, while the remaining $\delta n_i = 0$, giving

$$\dot{\phi}_k^2 = -6T \left[\frac{\mu_k + \mu_{k+1}}{\mu_k \mu_{k+1}} \right]. \tag{20}$$

Equation (20) determines the maximal fraction of kinetic energy $\dot{\phi}_k$ can possess. After this we numerically search for the maximum of V, subject to constrain that ϕ_k has a fixed value. This clearly gives the maximum of the negative kinetic energy available for the whole system. Equation

$$\max \{\dot{\phi}_k^2\} = \frac{6(\mu_k + \mu_{k+1})}{\mu_k \mu_{k+1}} \{V_{\max}(\phi_k) - E_0\} \tag{21}$$

defines the maximum velocity curve, where the energy constant is obtained from the initial conditions. In general, the curves are different for each separation angle, unless the masses are equal.

Figure 8 depicts phase space plots for some of the previous numerical experiments, together with corresponding maximum velocity curves. For small perturbation around the compact configuration, the curve encircles two separate regions, within which the motion is bound. The leftmost region constraints the interparticle separations ϕ_1 and ϕ_2, while the ϕ_3 is bounded inside the other region. These regions join together if E/V_I is increased to the above mentioned critical value 1.689, and then gradually widen. As can be seen in Fig. 8, a large portion of the allowed phase space is actually filled with trajectories, especially in the unstable case. However the joining of the two regions is not a sufficient condition for the motion to actually pass from one region to another. For the symmetric mode, the actual value of E/V_I for which the transition was observed, is about 0.6% larger than V_{III}/V_I. Clearly, the initial eigenmode is important: in the antisymmetric case the required E/V_I is about 6% larger. The reason for this mode dependence is evident from the $V(\alpha, \beta)$ plots: the oscillations must have a proper direction to facilitate the transition. Hénon (1970) found a similar kind of behavior in his study of Hill's problem. Retrograde, orbiting satellites about a planet remain in bounded orbits while prograde satellites, with the same energy, can leave the Hill's sphere and escape.

Equation (21) for the maximum velocity curve provides a convenient way to determine the energetically allowed minimum separation between satellites: for a given total energy, determine the ϕ_k for which the max $\{\dot{\phi}_k^2(\phi_k, E)\} = 0$. Figure 9 collects the observed minimum separations, $\phi_{\min}$, attained in integrations starting from Type I configuration with various initial E/V_I and perturbation modes, and compares these with the lower limit, ϕ_{mvc}, calculated from the above condition. Arrows indicate the

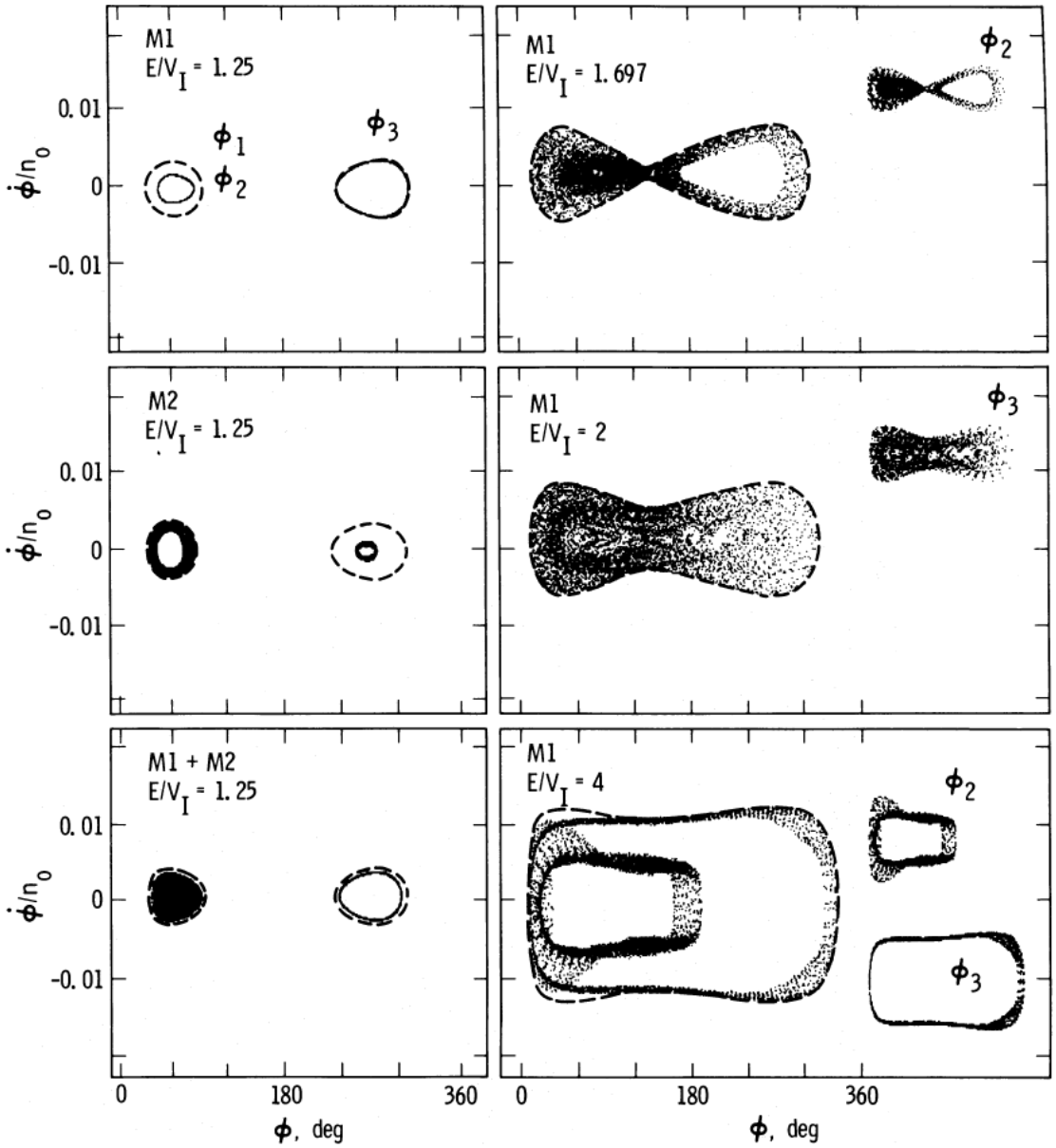

Fig. 8. Examples of phase space plots for $\phi_i = \theta_{i+1} - \theta_i$, together with the corresponding maximum velocity curves (dashed lines). Left panel compares $M1$, $M2$, and $M1 + M2$ modes for $E/V_I = 1.25$, while the right panel shows the behavior of initially symmetric perturbation ($M1$ mode) for larger E/V_I. The scale of the plots of the individual particle pairs is $\frac{1}{2}$ of the scale of the combined plot

onset of instability in our numerical integrations. This instability occurs for a $\phi_{\min}$ proportional to Hill's sphere of influence, defined by $\phi_{\text{Hill}} = \{(\mu_{k+1} + \mu_k)/3\}^{1/3}$. For identical satellites with $\mu = 10^{-5}$, $\phi_{\text{Hill}} = 1\overset{\circ}{.}12$. Notice that in the limit of large E/V_I the calculation of ϕ_{mvc} is simplified by the fact that at close approach, the gravitational energy can be approximated by the potential between the encountering pair:

$$V \sim -n_0^2\{\tfrac{1}{2}|\sin(\phi/2)|^{-1} - \cos(\phi)\} \sim -n_0^2/|\phi|\,.$$

Hence, for large E/V_I, $\phi_{\text{mvc}} \sim (E/V_I)^{-1}$.

For small perturbations, $E/V_I < 1.695$, the minimum distance depends strongly on the perturbation mode (Fig. 9b). In fact, for infinitesimal oscillation the combination $M1 + M2$ is optimal since it maximizes either ϕ_1 or ϕ_2, so that the system initially starts from the maximum velocity curve. However, for larger E/V_I, the initial conditions have less importance: the rapid drop in the observed $\phi_{\min}$ ($M1$ mode) corresponds to the above discussed transition from ordered to chaotic motion. According to Fig. 9, ϕ_{mvc} is a rather good approximation for $\phi_{\min}$ until $\phi_{\text{mvc}}/\phi_{\text{Hill}} \lesssim 6$ (for the mass ratio 10^{-5} this corresponds to $E/V_I = 5$). For larger E/V_I the energy formula derived from the simplified equations starts to fail, due to the non-Keplerian properties of orbits, leading to $\phi_{\min} < \phi_{\text{mvc}}$. Soon after this, somewhere between $E/V_I = 5.3$ and 5.5 (corresponds to $\phi_{\text{mvc}}/\phi_{\text{Hill}} \cong 5.2$ and 5.0, respectively), the close encounters lead to an escape to non-resonant orbits. In order to extend the obtainable range of E/V_I, a few integrations were carried out with $\mu = 10^{-7}$ (length of integration was 200,000 time units). In this case $\phi_{\text{Hill}} = 0\overset{\circ}{.}14$, and the resonance is again maintained until $\phi_{\text{mvc}}/\phi_{\text{Hill}} \approx 5$–6, corresponding to $E/V_I \approx 27$. It is interesting to note that the critical

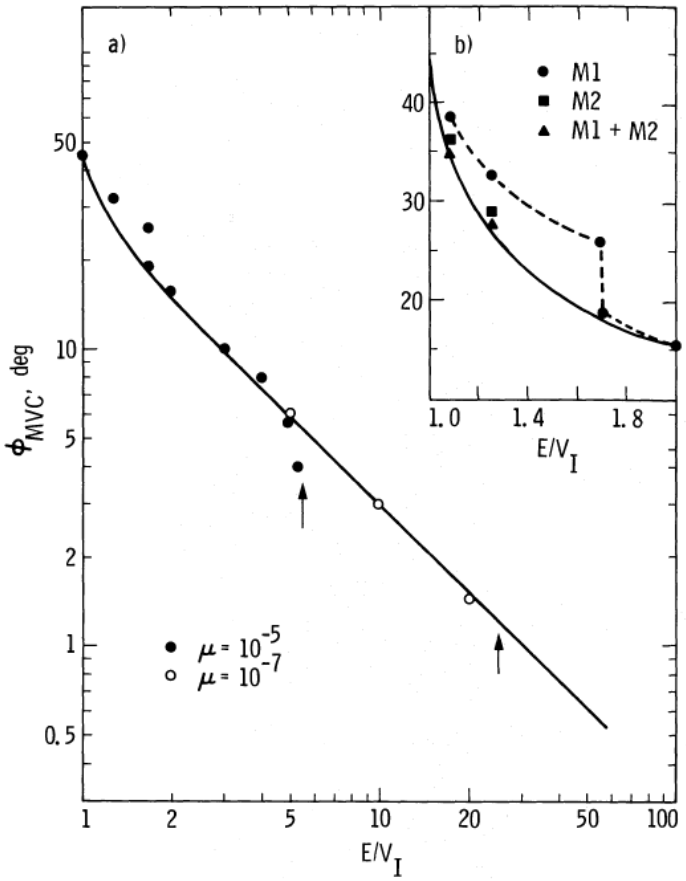

Fig. 9. The minimum separations observed in numerical integrations of three identical satellites, shown as a function of E/V_I. The minimum distances derived from Eq. (21) are shown by solid curves, while dashed lines connect observed separations. In (b) different modes are compared ($M1$: circles, $M2$: boxes, $M1 + M2$: triangles) for $E/V_I \leq 2$, while in (a) a larger range of E/V_I values is studied for the $M1$ mode. Two values of μ were investigated, $\mu = 10^{-5}$ (filled symbols) and 10^{-7} (open circles). Arrows indicate the E/V_I values which lead to global instability for these two values of μ

ϕ_{mvc} is in a very close agreement with the original instability criterion obtained by Maxwell (1890) for $N \to \infty$: if this is written in terms of the minimum separation, one finds $\phi_{cr} \approx 5.4\phi_{Hill}$. On the other hand, Dermott and Murray (1981) obtained $\phi_{cr} \approx 2.9\phi_{Hill}$ in numerical integrations for the $N = 2$ case. We shall return to effects of unequal masses on the minimum separations in Sect. 5.

We finally turn our attention to rings composed of more than three identical satellites. Although it is not possible to use potential plots to describe the motion, maximum velocity curves are readily applicable also for $N > 3$. Figure 10a shows an example of the different perturbation modes around the Type I stationary configuration, for $N = 5$ satellites (compare this with Fig. 5). The mode $M1$ corresponds to the symmetric expansion, which has the tendency to become unstable for the equidistant configuration. Indeed, when E/V_I is increased (Fig. 10b) this mode is the first one to lead to unstable behavior. It also mixes with the other three modes, and is mostly responsible for the spreading visible in these oscillations. Corresponding phase space plots are shown in Fig. 10c, together with the maximum velocity curves. Since in this case $E/V_I > V_{III}/V_I$, both regions of the phase space are connected. However, as in the case $N = 3$, the actual onset of chaos depends on the initial mode.

According to the eigenmode analysis, the behavior of the Type III stationary configuration changes its nature for $N > 6$ satellites. This is illustrated in Fig. 11, showing the time evolution in integrations of exact equations for $N = 3$ to 8 satellites. All the integrations start from the equidistant separations, with initial separations corresponding to the smallest eigenvalue (slowly evolving in-phase oscillations). In Fig. 11a the initial perturbation corresponds to kinetic energy $T = 10^{-5}(V_{II} - V_I)$, so that the particles start practically at rest. For Fig. 11b, $T = (V_{II} - V_I)$. As can be seen (Fig. 11a), with the small initial amplitude the $N = 7$ as well as $N = 8$ satellite rings perform only small oscillations around the equidistant positions. For $N \leq 6$ this configuration is clearly unstable, in the sense that satellites do not stay bounded to the vicinity of these positions. This result is in accordance with the predictions of the eigenmode analysis.

There is some difference in the qualitative behavior of slightly perturbed $N = 3$ and $4 \leq N \leq 6$ satellite rings (Fig. 11a): while the former case leads to a continuous exchange of orbits, for $N > 4$ the initially equidistant satellite ring can start to perform apparently stable, although large amplitude oscillations around the Type I configuration. The behavior can be visualized as follows. In the case $N = 3$ the potential was drawn as a function of α and β. For $N > 3$ there exists a corresponding $N - 1$ dimensional surface, defining the potential energy as a function of $N - 1$ independent difference angles. This potential has N maxima, each corresponding to Type I stationary solution centered at one of the particles. Now the system starts from the equidistant local minimum, and rapidly 'falls' to any one of these maxima. It is unable to return to the vicinity of the initial position, since its kinetic energy is rapidly divided between all the modes, including those corresponding to stable high frequency oscillations (for equally spaced $N = 3$ ring the two eigenmodes have the same time scale). Only occasionally (for example for $N = 4$ or 6) the system is able to find its way from one maximum to another. For $N = 7$ and 8 the equidistant solution is a local maximum, and the system can stay there if the excess kinetic energy is not too large.

If the perturbation is larger (Fig. 11b), the increase in the excess kinetic energy makes it impossible to stay in the vicinity of any single local maximum. Perhaps the most usual feature is the tendency for the particles to occasionally bunch together. The larger initial perturbation can also shift the stable $N = 7$ ring to a random wandering from the vicinity of one Type I configuration to another. For the same relative perturbation, the $N = 8$ ring stays around its initial configuration. The reason for this behavior is the small eigenvalue for the case $N = 7$, indicating that the local maximum corresponding to the equally spaced configuration has a very limited extent as compared to the case $N = 8$. The same is evident in Fig. 11c, showing the phase space plots together with the maximum velocity curves: for $N = 8$ the maximum velocity curve encircles two separate regions. In general, the maximum velocity curves give meaningful limits for the motion also in the case $N > 3$. However, although not so easy to see in small scale plots, the trajectories in the vicinity of the bounding curves seem to become slightly more sparse if N is increased.

A few additional integrations were performed for $N = 8$ and $N = 9$, in order to understand the qualitative consequences of

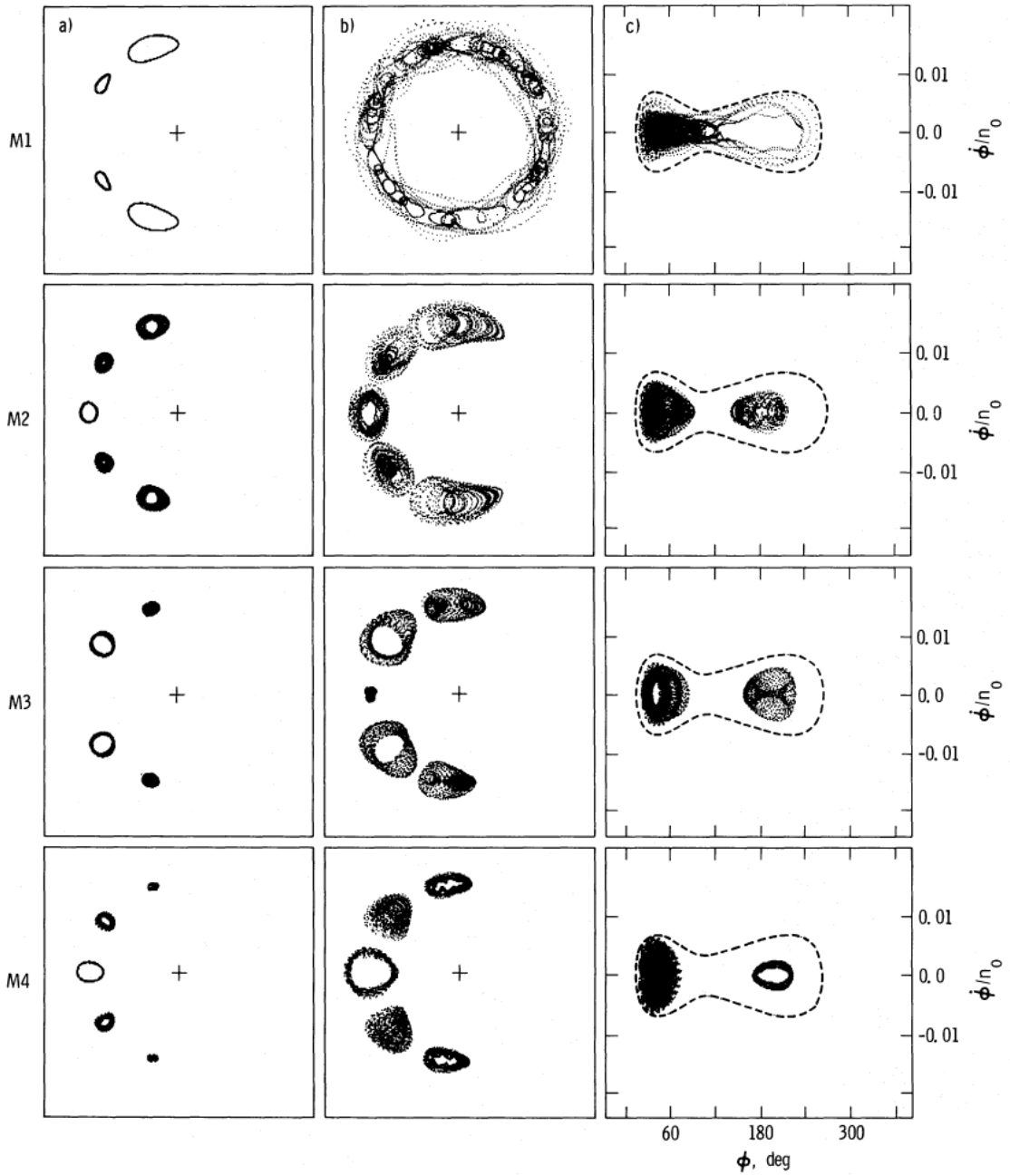

Fig. 10a–c. Numerical integrations for $N = 5$ identical satellites, starting from the Type I configuration with deviations corresponding to the four different eigenmodes ($M1 - M4$) (Compare with Fig. 5). In the polar plots (**a** and **b**) the radial deviations are scaled by factor 60: two perturbation amplitudes are studied: $E/V_1 = 1.05$ and 1.21. In **c** the combined phase space plots of the different modes for $E/V_1 = 1.21$ are shown, together with maximum velocity curves (dashed curves)

the disappearance of the more compact stationary configuration for $N = 9$. However it was very hard to see any qualitative difference in the behavior. This confirms the picture that the N Type I maxima and the one Type II maximum, which have already for $N = 8$ almost identical heights, gradually merge into one broad maximum for $N \geq 9$, without any drastic change in the characteristics of the dynamical system.

5. Unequal satellite masses

The previously explored case of N identical satellites is, although a necessary first step, not a very realistic model for any coorbital satellite system. For example, the coorbiter satellites of Saturn, Janus (S10) and Epimetheus (S11), have a mass-ratio $m_{S10}/m_{S11} \approx 3.6$ (Yoder et al., 1987). The other known examples, the tiny Lagrangian companions of Dione and Tethys, not to mention the Trojan asteroids, all involve a system where there is only one dominant satellite beside the primary. Therefore, we shall briefly explore some implications of nonequal masses, although only for $N = 3$ satellite ring. Much of the above discussion for identical satellites is valid also for the general case. For example, the three-particle potential has 3 local maxima, although in the general case they have unequal heights. Also, the stationary separations depend on the order of satellites: an ex-

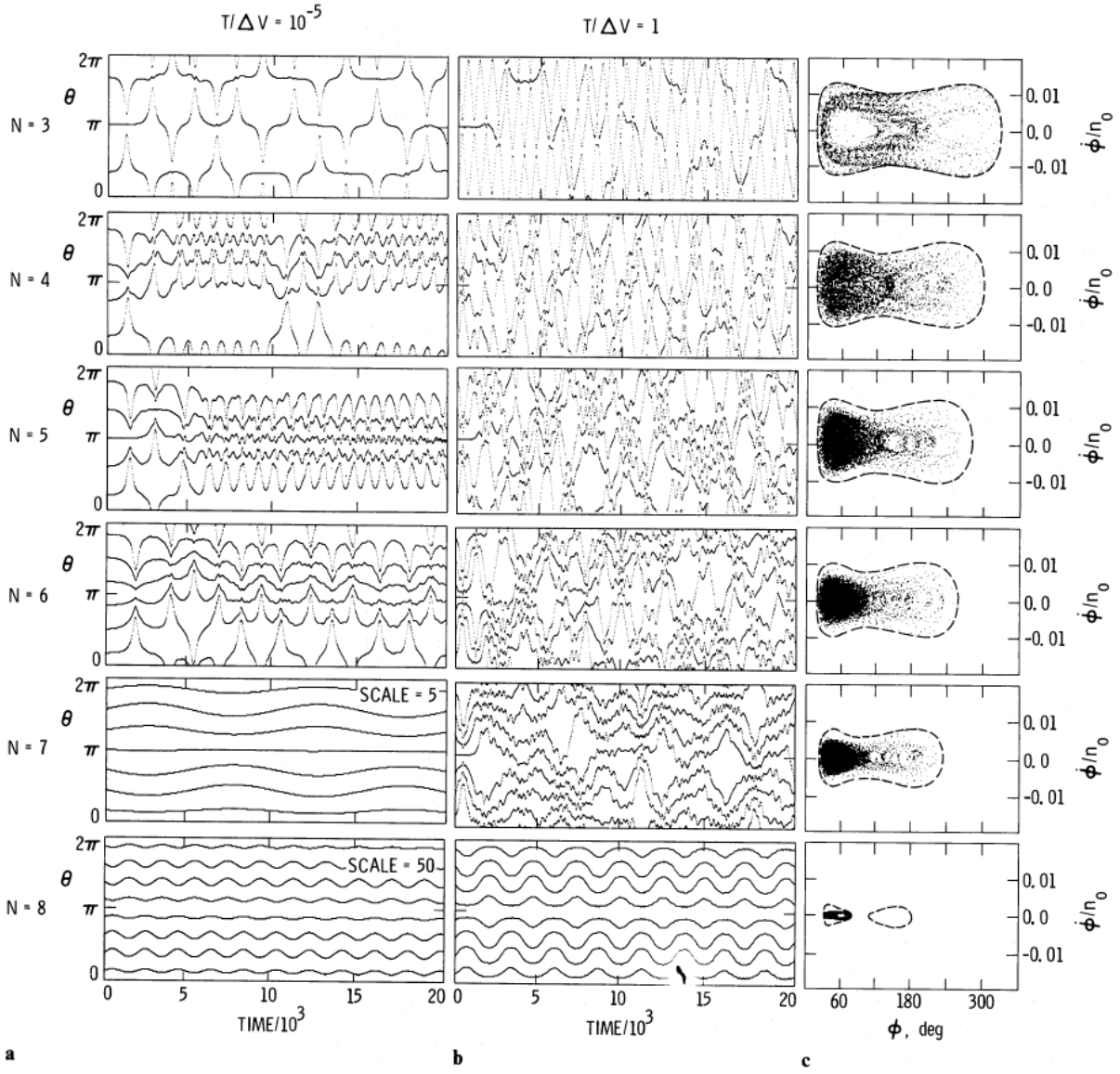

Fig. 11a–c. The evolution of a ring of $N = 3$ to 8 initially equally spaced satellites. The initial perturbation corresponds to the overall sinusoidal contraction of the ring (slowest eigenmode), with **a** $T = 10^{-5}\ \Delta V$ ($\Delta V = V_{II} - V_I$), or **b** $T = \Delta V$. The mass ratio is 10^{-5}, and the length of integration is 20,000 time units. In **c** the phase space plots, together with maximum velocity curves, are shown for the case (b)

ample is provided by Fig. 12, for relative masses $m_1/m_3 = 3.6$, $m_2 = 0.1(m_1 + m_3)/2$. The different stationary configurations are located at points $P_1 \to P_5$: P_1, P_2, and P_3 are local maxima, while P_4 and P_5 correspond to saddle points of V. Notice that the potential minimum, corresponding to equally spaced satellites in the case of identical masses, is not present. In fact, the local minimum vanishes if the masses differ more than about 10%.

According to Fig. 12, for small $|E|$ there exists three separate energetically allowed libration regions in the (α, β) plane, around positions P_1, P_2, and P_3. With increasing energy, two of them become connected, through P_4, corresponding to the horseshoe motion of the smallest mass with respect to the two massive satellites moving in mutual tadpole orbits. For still larger $|E|$, both remaining regions merge through P_5, allowing also for the mutual horseshoe orbits of the largest satellites.

Figure 13 depicts the results of a few numerical integrations performed with the relative masses studied in Fig. 12. Each calculation starts from the Type I stationary configuration around the smallest mass (P_2: $V_I = -0.513\mu^2 n_0^2 a_0^2$), and the initial perturbations satisfy: $m_1\,\delta n_1 = -m_3\,\delta n_3$; $\delta n_2 = 0$. This corresponds to the symmetric mode in the case of identical masses. The satellite to primary mass ratio is fixed by setting $\mu = \frac{1}{2}(m_1 + m_3)/M = 10^{-5}$, rather than the observed value of $\sim 10^{-8}$. Our choice speeds up the relative motion/mean orbit motion by a factor of ~ 30. The uppermost panel in Fig. 13 ($E/V_I = 2$) describes the libration of the large satellites, with the small satellite confined to move between them. Due to the unequal masses, the small satellite cannot remain stationary, but performs large oscillations. The second panel ($E/V_I = 2.3$) corresponds to the horseshoe orbit of m_2: in fact this value of E/V_I would allow for the mutual horseshoe orbit of the largest ones. However, in spite of the initial conditions m_1 and m_3 are immediately pushed to mutual libration. Only with enough large E/V_I (third panel, $E/V_I = 2.4$), the whole allowed (α, β) region is filled with trajectories.

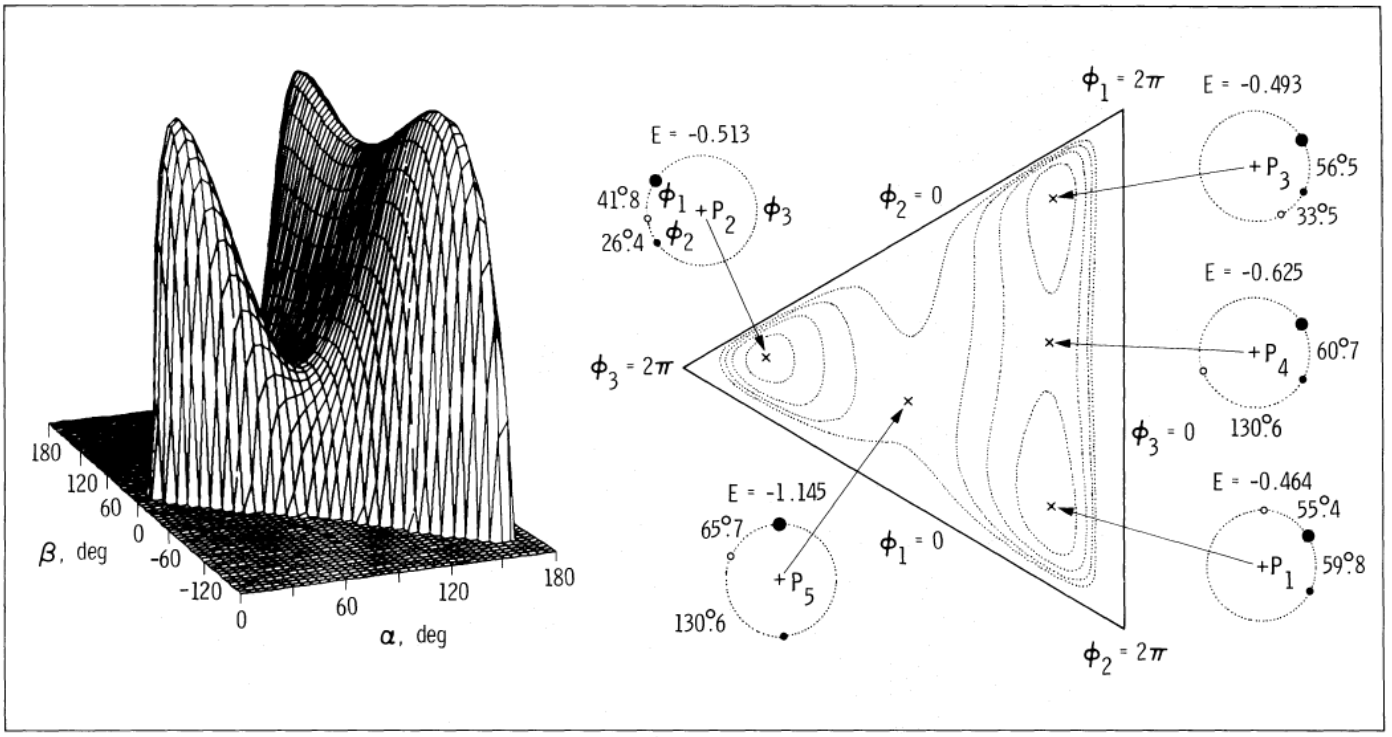

Fig. 12. A typical example of the 3 satellite potential in the case on nonequal masses ($m_1/m_3 = 3.6$; $m_2 = 0.1\,[m_1 + m_3]/2$). The interpretation of the (α, β) diagram in terms of the various stationary angular configurations is also shown. The energies of stationary separations $P_1 - P_5$ are given in units of $\mu^2 n_0^2 a_0^2$

It is clear from Fig. 13, that in the case of unequal masses, the motion of the smallest particle is less restricted than that of others. This is also evident from Eq. (21), where max $\{\dot{\phi}_k^2\}$ scales proportionally to $1/\mu_k$ if $\mu_k \ll \mu_{k+1}$. Similarly the minimum allowed distance scales $\sim \mu_k$ on the limit of large E/V_I. On the other hand, ϕ_{Hill}, involving the factor $(\mu_{k+1} + \mu_k)^{1/3}$ is not very sensitive to μ_k. This shows that the smallest satellites are at least in principle most prone to a close encounter and subsequent escape. Therefore, it is of interest to study in more detail how well the maximum velocity curves describe the actual limits of motion for the case of unequal masses.

Figure 14a depicts the theoretical minimum distance $\phi_{\text{mvc}}^{(k)}$ as a function of E/V_I, together with observed minimum separations, for the above mass ratios. Now each separation angle has its own minimum curve: the most important is the one for the separation between the smallest two satellites, $\phi_{\text{mvc}}^{(2)}$. Two mass ratios are studied, $\mu = 10^{-5}$ and 10^{-7} (integrations extend over 20,000 and 200,000 time units, respectively), yielding $\phi_{\text{Hill}}^{(2)} = 0.^\circ 69$ and $0.^\circ 15$, respectively, for the encounters between these two satellites. As in the case of identical satellites (see Fig. 9), for large E/V_I the actual minimum separations are fairly close to their theoretical lower bounds. In the integrations with $\mu = 10^{-5}$, $E/V_I = 2.4$ is the largest studied value still preserving the long term stability (no passing of satellites during about 20 oscillations), while $E/V_I = 2.5$ leads to an escape during the first few oscillations. The corresponding ϕ_{mvc}'s are $4.3\phi_{\text{Hill}}$ and $4.0\phi_{\text{Hill}}$. The integrations with $\mu = 10^{-7}$ bracketed the critical ϕ_{mvc} between 4.7 and $4.4\phi_{\text{Hill}}$. Therefore, the stability limit is about the same as for identical masses, namely $\phi_{\text{mvc}} \approx 5\phi_{\text{Hill}}$.

It is clear that the theoretical lower bound cannot be applicable in the case of very large relative mass ratios; in the test particle limit Eq. (21) certainly breaks down. The time scale to attain the bounding values is also expected to increase with decreasing μ. In order to study how well the agreement between ϕ_{mvc} and ϕ_{min} holds true for very unequal masses, a few additional integrations were performed with decreased m_2 (Fig. 14b). The perturbation was fixed by $E/V_I = 3$, while $\mu = 10^{-7}$. The minimum separations were found to follow closely their theoretical lower bounds, until $m_2/M = 0.015\mu$, in which case the observed minimum distance was clearly above the theoretical lower bound, indicating that the timescale to attain boundaries exceeds the length of integration (200,000 time units). However, for $m_2/M = 0.012\mu$ the system became unstable, in accordance with what would be expected from the previous experiments (corresponds to about $\phi_{\text{mvc}} \approx 3\phi_{\text{Hill}}$). Due to the limitations of numerical integrations larger relative mass differences were not studied, and no attempt was made to determine the exact timescale of reaching the minimum separations as a function of m_2.

According to these numerical experiments minimum separations derived from Eq. (21) agree with the actually attained separations, at least as long as the masses do not differ more than about a factor of ~ 100. These results can be related to the Saturn's coorbiter pair as follows. Assume $m_{S10}/M_{SAT} = 6.5\,10^{-9}$, and $m_{S10}/m_{S11} = 3.6$ (Yoder et al., 1987). These mass values combined with the observed mean motion $n_0 = 518.^\circ 3$/day, and the maximum of differential angular velocity, $\dot{\phi}(60^\circ) = 0.^\circ 26$/day (Yoder et al., 1983), imply $E/V_I \approx 37$. Figure 15 studies the theoretical minimum separation between Epimetheus (S11)

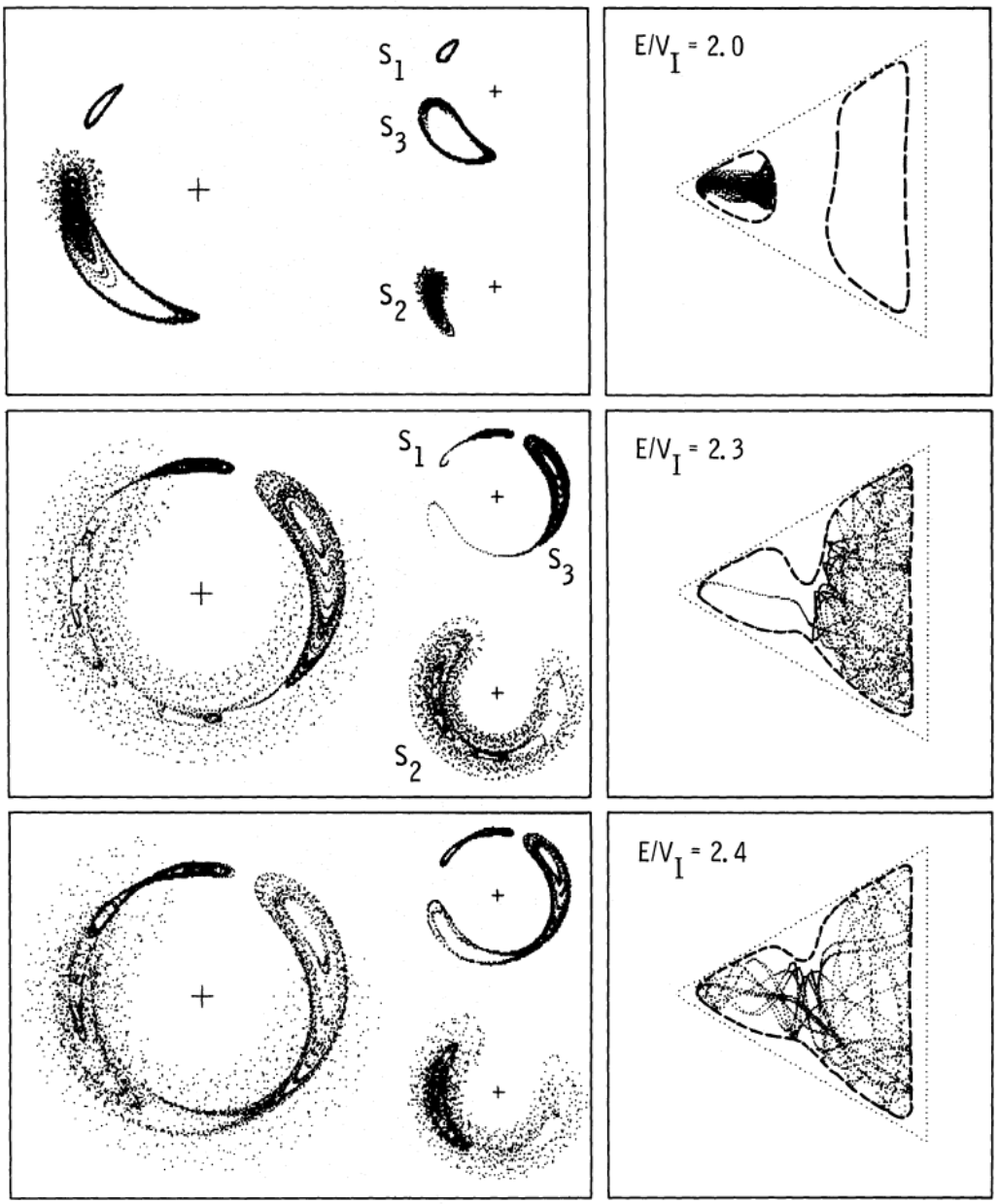

Fig. 13. Numerical integrations with unequal masses. The relative mass ratios are the same as in Fig. 12, and $\mu = 10^{-5}$. Integrations start from Type I configuration around the mass m_2 ($V_1 = -0.513$). Three values of E/V_1 are studied (2, 2.3, and 2.4)

and a hypothetical third body with mass m_T, as a function of E/V_0, where V_0 is the potential energy for 60° separation between S10 and S11. If the stability limit $\phi_{mvc} \approx 5\phi_{Hill}$ is valid, Fig. 15 implies that unless $m_T > 0.3\, m_{S11}$, the system would be unstable for the present total energy. However, a less massive third body could be stable if E/V_0 were reduced. For example, for the limiting tadpole orbit ($E/V_0 = 3$), the minimum allowed m_T would be about $0.013 m_{S11}$. For smaller m_T, its motion could become unstable if large particles were performing large tadpole orbits. However, in the limit of vanishing kinetic energy, librations around Type I configuration are expected to be stable even for a massless test particle.

The above limit for m_T, however, is even roughly valid only if the free orbital eccentricities are ignored. For example, according to Eq. (21) the minimum separation between S10 and S11 is ~8°, or about $100\phi_{Hill}$. Due to the substantial eccentricities ($e_{S10} = 0.007$, $e_{S11} = 0.009$; Synnott et al., 1983) the actual minimum separations can vary by about ±2°. Since $5\phi_{Hill} \ll 2°$, the variation in fact approximates the critical minimum separation. The same is true if a third particle is added: for close encounters between Epimetheus and a body with similar mass $\Delta\phi_{min} \approx 1°$ or $\approx 15\phi_{Hill}$, even if the latter is assumed to have zero eccentricity. According to Fig. 15, if the three particles system had the same energy as is present in the coorbiter pair, then the minimum separation of this massive third body with Epimetheus is less than $15\phi_{Hill}$ and hence is forced to a crossing orbit with Epimetheus. Therefore, if we assume that S10 and S11 represent the upper end of the size distribution of the fragments

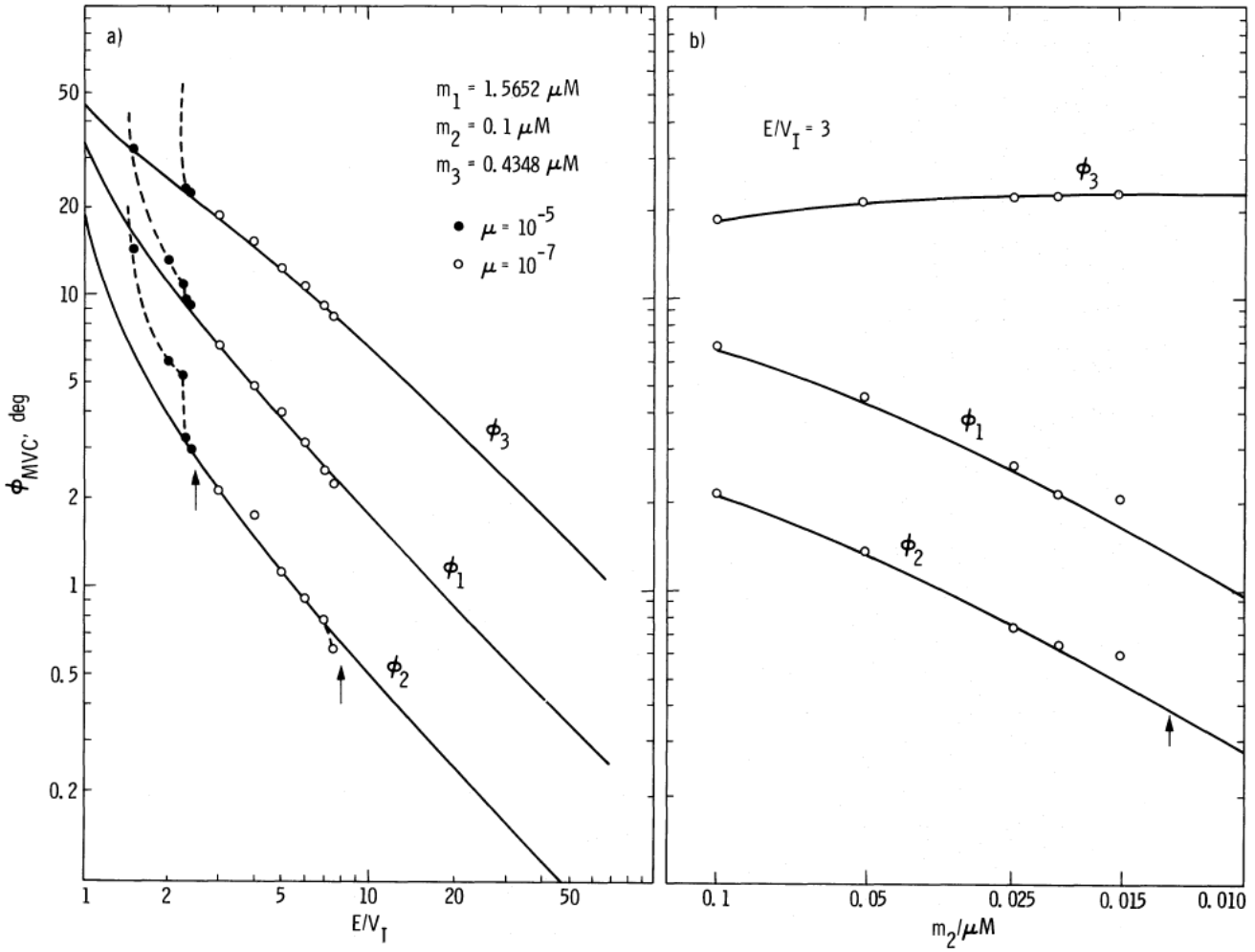

Fig. 14. a The observed (circles) and theoretical minimum distances (solid curves) for the relative masses of Fig. 13. Each separation is plotted separately, as a function of E/V_I. Filled circles represent integrations with $\mu = 10^{-5}$, while for open circles, $\mu = 10^{-7}$. Arrows indicate E/V_I values which lead to instability, for these two values of μ. **b** The same as (a), except that m_2 is given values between 0.1 and $0.01(m_1 + m_3)/2$, for a fixed $E/V_I = 3$

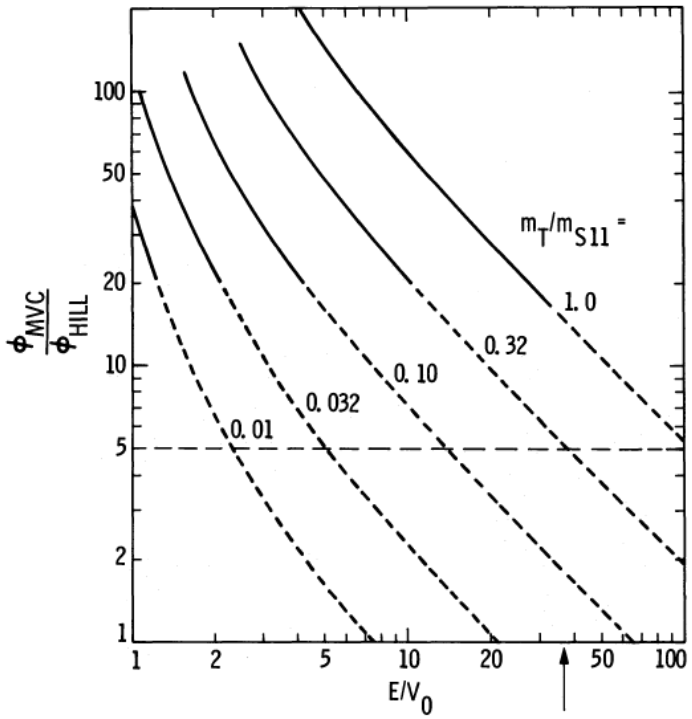

Fig. 15. The theoretical minimum separation ϕ_{mvc}, in units of ϕ_{Hill} for a system consisting of Janus (S10), Epimetheus (S11), and a third mass m_T, as a function of E/V_0, where V_0 is the potential energy for 60° separation between S10 and S11. Only the minimum separation between S11 and third body is shown, for different mass ratios m_T/m_{S11}. The approximate critical limit for circular case, $\phi_{mvc} = 5\phi_{Hill}$, is shown by vertical line, while the dashed portion of the curves indicate $\phi_{mvc} < 1°$. Arrow at $E/V_0 = 37$ denotes the estimate for the present energy of the coorbital pair

of a primordial satellite which has suffered a catastrophic impact, it seems plausible that all the other fragments except Janus and Epimetheus have been ejected to non-resonant orbits and were removed by collision or ejection from the Saturnian system. The formation of a triplet would apparently require very fortuitious initial conditions. However, the origin and stability of the co-orbiter pair may have been critically affected by this ejection process. This hypothesis and other explanations for their origin requires further study.

6. Conclusions

A reasonably thorough examination of the coplanar, nearly circular particle rings with $N \leq 9$ satellites has been performed, using a combination of simplified and exact dynamical equations. The determination of various stationary configurations, their eigenfrequencies and eigenmodes, was obtained from a numerical search of the simplified equations and the stability matrix for infinitesimal oscillations. The behaviour of the system for finite oscillations was explored numerically with both sets of equations, and we found little difference in the qualitative results.

The few particle ring (with equal masses) has three distinct stationary configurations. The most important one, a closely packed configuration (Type I) where all the particles tend to clump on one side of the mean orbit, exists for $N \leq 8$, and is stable to small oscillations. The equally spaced configuration represents a local minimum in the potential energy for $N \leq 6$ and is thus unstable. For $N \geq 7$ it becomes stable: for $N \geq 9$ all the maxima merge, and the equally spaced configuration is the only stationary solution. Most of our studies were concentrated on the behaviour of $N = 3$ ring when perturbed from its stable configuration.

For the ring of 3 identical masses, the two eigenmodes are symmetric and antisymmetric in the relative velocity of the central particle with respect to its neighbours. In the symmetric mode, the central particle is nearly stationary and the remaining satellites move towards or away from it, while in the antisymmetric mode it starts to deviate towards either of the other satellites. For small oscillations, these modes (especially the initial strictly symmetric mode) tend to remain distinct, but they increasingly couple as energy is increased. Possibly the most interesting result of this study was the discovery of strongly chaotic motion, which becomes possible once the energy exceeds a critical value $E/V_I \geq V_{III}/V_I$. This critical energy could be predicted from the *maximum velocity curve*, which bounds the differential velocity versus separation of a given pair of particles. The onset of chaos appears to occur with the merging of two distinct maximum velocity curves, within which the motion is more regular. We found that the collective histories of identical particles tend to fill the available phase space all the way to the boundary once chaos set in, but also that the passage to chaos tended to occur first for the initially symmetric modes as energy was increased just past E_{cr}. For the antisymmetric mode, the onset occurred for a slightly larger energy. Thus it appears that the onset of chaos for our problem depends not only on the energy, but also on the initial conditions, or more to the point, the initial eigenmode of the system.

The maximum velocity curves were used to deduce the minimum separations between pairs of satellites (for the $N = 3$ case, although the method is applicable also to $N > 3$). Numerical experiments indicate that for large E/V_I, when the motion has a chaotic nature, the particles sooner or later came very close to the minimum values, regardless of the initial perturbation mode. On the other hand for extremely large E/V_I the observed minimum separation can be smaller than the predicted one, since the basic assumptions of the simplified description are no longer valid. However, it was observed that generally the theoretical minimum separations are a very good indicator of the global stability of the 1:1 resonance: once the calculated minimum separation becomes comparable to about 5 times the Hill's sphere of influence, the close encounters rapidly destroy the resonance.

Application to the coorbiter pair of Saturn, Janus and Epimetheus, seems to indicate that even in the hypothetical case of circular orbits, no stable motion would be possible for a third resonant satellite with less than about 10% of the combined mass of S10 and S11 (assuming the present total energy of the S10-S11 pair). This inspite of the fact that the coorbital pair itself is safely in the stable region. If the actual eccentricities are taken into account, it can further be deduced that even a triplet with S10 and two masses of the size of S11 would be unstable. This seems to offer at least a preliminary explanation why there is no examples of true $N = 3$ satellite rings, at least not with the high E/V_0 ratios. However, a detailed model for the formation of the coorbital satellites would be very desirable.

Acknowledgements. This paper presents the results of one phase of research carried out at the Jet Propulsion Laboratory, California Institute of Technology, under contract to NASA. H. Salo was supported by the National Research Council and the Finnish Academy of Sciences.

References

Brown, E.W., Shook, C.A.: 1964, *Planetary Theory*, Dover, New York

Dermott, S.F., Murray, C.D.: 1981, *Icarus* **48**, 1

Hénon, M.: 1970, *Astron. Astrophys.* **9**, 24

Maxwell, C.J.: 1890, *On the stability of the motion of Saturn's Rings*, in Scientific Papers of James Clerk Maxwell, Cambridge University Press, Vol. **1**, 228

Pendse, C.G.: 1935, *Phil. Trans. Roy. Soc. London* (*A*) **234**, 145

Synnott, S.P., Peters, C.F., Smith, B.A., Morabito, L.A.: 1981, *Science* **212**, 191

Yoder, C.F., Colombo, G., Synnott, S.P., Yoder, K.A.: 1983, *Icarus* **53**, 431

Yoder, C.F., Synnott, S.P., Salo, H.: 1987, *Bull. Amer. Astron. Soc.* **19**, 896

Willerding, E.: 1986, *Astron. Astrophys.* **161**, 403